PNAS

Supporting Information for

Changes in patterns of age-related network connectivity are associated with risk for schizophrenia

Roberta Passiatore[a,b,c], Linda A. Antonucci[a], Thomas P. DeRamus[b], Leonardo Fazio[d], Giuseppe Stolfa[a], Leonardo Sportelli[a], Gianluca C. Kikidis[a], Giuseppe Blasi[a,e], Qiang Chen[f], Juergen Dukart[c,g], Aaron Goldman[f], Venkata S. Mattay[f,h], Teresa Popolizio[i], Antonio Rampino[a,e], Fabio Sambataro[j], Pierluigi Selvaggi[a,e], William Ulrich[f], Apulian Network on Risk for Psychosis[a,k,l,m,n,o], Daniel R. Weinberger[f], Alessandro Bertolino[a,e*], Vince D. Calhoun[b*], Giulio Pergola[a,f,p*]

[a] Department of Translational Biomedicine and Neuroscience – University of Bari Aldo Moro, Bari, IT.
[b] Tri-institutional Center for Translational Research in Neuroimaging and Data Science (TReNDS) – Georgia State University, Georgia Institute of Technology, and Emory University, Atlanta, GA, USA
[c] Institute of Neuroscience and Medicine, Brain & Behavior (INM-7), Research Centre Jülich, Jülich, DE
[d] Department of Medicine and Surgery - LUM Jean Monnet, Casamassima, IT
[e] Psychiatric Unit - University Hospital, Bari, IT
[f] Lieber Institute for Brain Development – Johns Hopkins Medical Campus, Baltimore, MD, USA
[g] Institute of Systems Neuroscience, Medical Faculty, Heinrich Heine University Düsseldorf, Düsseldorf, DE
[h] Department of Neurology and Radiology – Johns Hopkins Medical Campus, Baltimore, MD, USA
[i] Neuroradiology Unit - IRCCS Casa Sollievo della Sofferenza Hospital, S. Giovanni Rotondo, IT
[j] Section of Psychiatry, Department of Neuroscience - University of Padova, Padua, IT
[k] Department of Mental Health, ASL Foggia, Foggia, IT
[l] Department of Clinical and Experimental Medicine, University of Foggia, Foggia, IT
[m] Department of Mental Health, ASL Barletta-Andria-Trani, Andria, IT
[n] Department of Mental Health, ASL Bari, Bari, IT
[o] Department of Mental Health, ASL Brindisi, Brindisi, IT
[p] Department of Psychiatry and Behavioral Sciences, Johns Hopkins University School of Medicine, Baltimore, MD, USA

*Please, address correspondence to:

Giulio Pergola
Address: Piazza Giulio Cesare, 11- 70121 Bari, Italy
Phone: +39 080 5478548 - E-mail: giulio.pergola@uniba.it

Vince D. Calhoun
Address: 55 Park Place - 30303 Atlanta, GA, USA
Phone: +1 505 514-5850 - E-mail: vcalhoun@gsu.edu

Alessandro Bertolino
Address: Piazza Giulio Cesare, 11 - 70121 Bari, Italy
Phone: +39 080 5478572 - E-mail: alessandro.bertolino@uniba.it

This PDF file includes:

Appendix. Supporting Information

1. Sample determination: exclusion criteria and quality check process

For this study, we analyzed data from a total of 9236 individuals included in six different cohorts acquired at the Lieber Institute of Brain Development (LIBD), at the University of Bari Aldo Moro (UNIBA), included in the Philadelphia Neurodevelopmental Cohort (PNC), in the Adolescent Behavior Cognitive Development^{SM} (ABCD) cohort, and the UK Biobank (UKB) cohort. Data for the UNIBA cohorts have been acquired at the same site through two different MRI scanners. As the experimental protocols were the same but the scanner differed, we considered acquisition from the two scanners separately (UNIBA1 and UNIBA2). We characterized nine different groups: neurotypical children (cNC=3726), i.e., individuals between 8 and 14 years old, children with at least one first-degree relative (parent or sibling) with schizophrenia (cFHR/SIB=62), children with subthreshold psychotic symptoms (cPSY=1284), younger neurotypical adults (yNC, N=757), i.e., individuals between 15 and 25 years old, younger siblings (SIB) of patients with schizophrenia (SCZ) (ySIB, N=53), younger individuals with subthreshold psychotic symptoms (yPSY, N=125, older neurotypical adults (oNC, N=2948), i.e., individuals older than 30 years old, older SIB (oSIB, N=87) and older patients with schizophrenia (oSCZ, N=195). No PSY met the age criterion to be qualified as an older PSY, i.e., PSY older than 30 years old.

For the UNIBA cohorts (UNIBA1 and UNIBA2), the experimental protocol was approved by the institutional ethics committee of the University of Bari Aldo Moro. Written informed consent was obtained after a full understanding of the protocol according to the Declaration of Helsinki. For the LIBD cohort, the experimental protocol was approved by the National Institutes of Health research committees. For PNC, all study procedures were approved by the Institutional Review Board at the University of Pennsylvania. Most ABCD research sites rely on a central Institutional Review Board at the University of California, San Diego for the ethical review and approval of the research protocol, with a few sites obtaining local IRB approval. UKB received ethical approval from the Research Ethics Committee (reference 11/NW/0382).

LIBD, UNIBA 1 and UNIBA 2. All participants were assessed in person with a Structured Clinical Interview for Diagnostic and Statistical Manual of mental disorders version IV (DSM IV) (1). Exclusion criteria for neurotypical participants included the presence of a DSM IV Axis I diagnosis at the time of the study and by history, having a first-degree relative with a psychiatric disorder, IQ < 80, recent drug or alcohol abuse (within 1 year), or >5 years of previous abuse, and current psychotropic pharmacological treatment. The SIB condition was defined by the absence of DSM IV Axis I diagnoses, with the contemporary presence of a first-degree relative affected by a DSM IV Axis I diagnosis. The exclusion of any psychiatric diagnosis for both NC and SIB was assessed with the SCID. The PSY condition was defined by cognitive disturbances (COGDIS), as assessed by (i) the Schizophrenia Proneness Instrument (SPI-A), and/or (ii) by satisfying the ultra-high-risk criteria for psychosis, according to the Structured Interview for Psychosis-Risk Syndromes criteria (SIPS). PSY were excluded when they had an intake of antipsychotic medication for more than 30 cumulative days, and when they had any intake of antipsychotic medication within the past 3 months before study enrollment.

PNC. The Philadelphia Neurodevelopmental Cohort (PNC) is a large-scale study of child development that combines neuroimaging, diverse clinical and cognitive phenotypes, and genomics (https://www.med.upenn.edu/bbl/philadelphianeurodevelopmentalcohort.html). We focused on participants between 8 and 23 years of age for whom we recorded both youth self-rating and caregiver ratings on a spectrum of psychopathology symptoms. Caregivers were either

mothers (~86%), fathers (~10%), or other family members/legal guardians (~3%). Refer to Calkins*, et al.* (2) for details on study design, recruitment, and other procedures for the PNC study. Briefly, written assent from youths and written informed consent from caregivers were obtained after they received a description of the study procedures. Youths and caregivers were assessed separately. All participants were informed of the confidentiality of the reports, except for required reporting in cases of suicidal ideation, suicidal intent, and/or abuse. Individuals and caregivers rated lifetime psychopathology symptom items on the computerized version of GOASSESS (2), a structured interview and assessment that incorporates well-validated and reliable measures for psychopathology screening, evaluating (i) psychopathology symptoms, (ii) their frequency, duration, distress and/or (iii) impairment associated with psychopathology domains, in addition to (iv) treatment history and the lifetime prevalence of any disorder. Psychopathology measures in GOASSESS include the following measures: (a) the NIMH Genetic Epidemiology Research Branch Kiddie-Schedule for Affective Disorders and Schizophrenia (K-SADS) is an extensively validated widely used, highly reliable measure considered to be the "gold standard" to assess DSM psychopathology symptoms; (b) the revised PRIME screen for assessment of positive sub-psychosis symptoms, a measure with high internal consistency, Cronbach's alpha of 0.88, and high sensitivity and specificity, respectively of 1.00 and 0.74 (3); (c) Scale of Prodromal Syndromes (SOPS) which assesses negative and disorganized psychotic symptoms with high internal consistency, Cronbach's alpha 0.85 (4). For this study, we selected 113 symptom items from GOASSESS that were consistently reported in the overall sample as described by Xavier*, et al.* (5). These 113 items corresponded to symptom items from 14 different psychopathological. These domains included attention deficit hyperactivity, agoraphobia, conduct, generalized anxiety, depression, mania, obsessive compulsive, oppositional defiant, panic, specific phobias, psychosis, separation anxiety, social anxiety, and post-traumatic stress disorder. One hundred and three of the 113 items were discrete, coded with a '1' for 'presence' and '0' for 'absence'; unknown responses were re-coded to 0 since we use sum scores for all analyses; recoding values to 0 has shown to have little to no effect on validity (6). Twelve items were Likert-type questions with 7 possible values ranging from 'definitely agree' = 6 to 'definitely disagree' = 0. The individual psychopathology symptom domain score was calculated as the sum of all item responses for each psychopathology domain. Symptoms items for the psychosis spectrum include suspiciousness or odd ideas of reference, odd or bizarre ideas that are not delusional, unusual or eccentric behavior, unusual perceptual experiences that are not psychotic, disorganized or odd speech, inappropriate affect, hallucinations or delusions (sub-threshold), and passivity experiences. All the symptoms assessed, psychopathological domains, and the number of symptom items per domain are available at https://osf.io/v4wj5/. Since the number of items varied by domain, individuals who reported one or more symptoms for a specific psychopathological domain were assigned a score of 1, while who indicated no symptoms were assigned a score of 0 in that psychopathological domain. Individuals who scored 0 in all psychopathological domains were classified as neurotypical (NC). Individuals who scored > 1 in the psychosis spectrum domain were identified as individuals with subthreshold psychotic symptoms (PSY). Individuals who scored > 1 in at least one of the other psychopathological domains except psychosis were excluded from the analysis.

ABCD. This is a multisite, longitudinal study designed to recruit more than 10,000 children aged 9-10 and follow them over 10 years into early adulthood (https://abcdstudy.org/). The parent's full written informed consent and the child's assent were obtained under protocols approved by the Institutional Review Board. Participants and their caregivers completed a wide assessment including both physical and mental health information. We derived family mental health history information from the Family History Assessment Module Screener (FHAM-S) (7) filled out by parents or caregivers. We characterized a group of individuals with at least one first-degree relative presenting schizophrenia-related symptoms, i.e., individuals at familial risk for schizophrenia

including siblings of patients with schizophrenia (cSIB/FHR). Also, the ABCD Prodromal Psychosis Scale and the KSADS-5 (8) have been used to assess parent-report of youth mental health as well as youth's self-report. We included individuals with >1 on the ABCD prodromal Psychosis Scale, following the same criterion to define PSY individuals in PNC (5), and with >1 at the reported psychotic symptoms at KSAD-5 as described by Karcher*, et al.* (9). Children without any clinical and sub-clinical psychiatric conditions, neurodevelopmental disorder, and/or central nervous system disorder have been included in the neurotypical group (cNC). We only included data at the baseline.

UKB. This cohort comprises around 500,000 community-dwelling participants recruited from across the United Kingdom of Great Britain and Northern Ireland between 2006 and 2014 (https://www.ukbiobank.ac.uk). A subset of around 50,000 participants who were part of the initial recruitment attended for head MRI scanning at an average of around four years after the initial visit. Participants completed a wide assessment through web-based questionnaires sent regularly after the first assessment including physical and mental health. Individuals were included in the absence of psychiatric symptoms including mental distress, depression, mania, anxiety, addictions, alcohol use, cannabis use, unusual and psychotic-like experiences, traumatic events, and self-harm behavior (Category 136). Those participants who had any psychiatric-related admissions were excluded from our analysis (Data-Field: 20544). oSCZ were not included in the present study due to the small number of individuals for which data were available (N=18). Individuals with neurological and central nervous system disorders were not included, as well. We included in our sample only individuals between 40 and 60 years old that are comparable with the oNC group in the other cohorts. All participants provided informed consent (http://biobank.ctsu.ox.ac.uk/crystal/field.cgi?id=200).

In all cohorts, we included participants with no history of head trauma with loss of consciousness, metal implants, or substantial medical or neurological conditions. Women of fertile age were included only with a negative pregnancy test. The sample size of individuals included in our analysis grouped by age, risk, and diagnosis, ie., cNC, cSIB/FHR, cPSY, yNC, ySIB, yPSY, oNC, oSIB, and oSCZ for each session for each cohort is reported in Table S1.

1.1 Age differences within and across cohorts

Age differences across groups at the same age stage within cohorts, i.e., cNC vs cPSY in the PNC; yNC vs ySIB in the LIBD, UNIBA1, and UNIBA2 cohorts, oNC vs oSIB, oNC vs oSCZ, and oSIB vs oSCZ in the LIBD and UNIBA1 cohorts; yNC vs yPSY in the UNIBA2 and PNC cohorts, have been assessed through separate Welch two-sample t test (Figure S1). Also, age differences between cohorts have been assessed through separate Welch two-sample t test. We found that cNC and cPSY were significantly younger in the ABCD compared with PNC (t=-7.74, p-value = 1.4×10^{-05}; t=-6.2, p-value = 2.2×10^{-06}); yNC were significantly younger in the PNC compared to the other three cohorts (PNC vs UNIBA1: t= -8.71, p-value = 2.2×10^{-06}; PNC vs UNIBA2: t= -7.9, p-value = 2.2×10^{-06}; PNC vs LIBD: t= -9.54, p-value = 2.5×10^{-06}); oNC in LIBD were significantly older than oNC in UNIBA1 (t = 2.45, df = 260, p-value = 0.01), and oNC in UNIBA2 (t = 2.8, df = 260, p-value = 0.008), as well as oSCZ in LIBD, were significantly older than oSCZ in UNIBA1 (t = 2.24, df = 260, p-value = 0.03) and in UNIBA2 (t = 2.23, df = 260, p-value = 0.03); yPSY in the PNC were significantly younger than yPSY in UNIBA2 (t = 5.03, df = 260, p-value = 1.2×10^{-06}). Finally, UKB oNC were significantly older that the LIBD, UNIBA1, and UNIBA2 (t=14.10, p-value = 2.2×10^{-16}; t=21.89, p-value = 2.2×10^{-16}; t=15.10, p-value = 2.2×10^{-16}). Age distributions are depicted in Figure S1. Given the substantial age differences, further analyses were corrected for age differences within age-stages.

2. Experimental fMRI protocols

The experimental protocol acquired for each cohort included resting state and different task-related acquisitions tapping onto the same cognitive domains (Table S2). For the LIBD and UNIBA1 cohorts, the experimental procedure was composed of a resting state, a blocked paradigm of the N-back task (10, 11), which measures increasing working memory loads, a blocked paradigm of an incidental declarative memory task, i.e., the Picture Encoding and Retrieval task (PEAR) (12-14), which dissociates specific encoding and retrieval processes. For the LIBD cohort, we acquired a block design implicit emotion recognition task, i.e., the Faces Matching task (FMT) (15), while for the UNIBA1 cohort, we used an event-related implicit emotion recognition task based on gender recognition in human faces - Faces (16). For the UNIBA2 cohort, the experimental procedure was composed of a resting state, a blocked paradigm of the N-back task (10, 11), which was the same as the one acquired for the other two cohorts, an event-related paradigm of an explicit associative memory task, i.e., a revised version of the Relational and Item Specific task (RISE) (12), which dissociate specific encoding and retrieval processes, and a revised version of the Faces task, used in the UNIBA1 cohort (17). For the PNC cohort, the experimental procedure was composed of a resting state, a fractal version of the standard N-back task (18), and an explicit emotion identification task (Emo) (19). For ABCD, the experimental procedure was composed of four short resting state sessions, and a revised version of the N-back task with emotional stimuli (20, 21). ABCD data were collected with 29 different scanners across 21 sites. See SI, Section 4 for data harmonization procedures. Finally, UKB included a resting state and the same emotion recognition paradigm used in LIBD, i.e., FMT (15). All UKB data presented in this study were collected on the same scanner.

Neuropsychological paradigms presented for each cohort are summarized in Table S2. Stimuli were presented via a back-projection system, and behavioral responses were recorded through an optic fiber response box to measure accuracy (the count of correct responses) and reaction time (RT, ms) for each trial. All subjects were trained on the tasks before the fMRI session.

2.1. Resting state

During each resting state fMRI, participants were instructed to remain awake, with eyes open, and fixate on the crosshair in the middle of a white screen (22, 23), as this is suggested to facilitate network delineation compared to eyes-closed conditions (24).

2.2. Working memory task

N-back task (LIBD, UNIBA1, and UNIBA2): During the working memory (WM) fMRI session, participants completed a blocked paradigm of the N-back task (10). The stimuli consist of numbers (range of 1-4) shown in random sequence and displayed in four corners of a diamond-shaped box. The task included a non-memory-guided condition (0-back), which presented the same stimuli but simply required subjects to identify the currently visible stimulus and a WM condition where subjects were required to recollect two (2-back) stimuli seen beforehand while continuing to encode additional incoming stimuli. The task alternated four 30-s blocks of a 0-back condition with four 30s blocks of the 2-back WM condition. We classified performance based on correct response during each working memory recollection block. We averaged the Hit count, reflecting the accuracy in terms of working memory performance. Individuals with a Hit rate<25% were excluded (25). Reaction time (RT) has also been extracted. Individuals with RT<200ms were excluded (11).

Fractal N-back task (PNC): During the working memory fMRI session, participants completed a fractal version of the standard N-back task (18). The task was chosen because it is a reliable probe of the executive system and has the advantage of not being contaminated by lexical processing abilities that also evolve during development (26). The task involved the presentation of complex geometric figures (fractals) for 500ms, followed by a fixed interstimulus interval of 2500ms. This occurred under three conditions: 0-back, 1-back, and 2-back, producing different levels of WM load. In the 0-back condition, participants responded with a button press to a specified target fractal. For the 1-back condition, participants responded if the current fractal was identical to the previous one; in the 2-back condition, participants responded if the current fractal was identical to the item presented two trials previously. Each condition consisted of a 20-trial block (60 s); each level was repeated over three blocks. The target-foil ratio was 1:3 in all blocks with 45 targets and 135 foils overall. Visual instructions (9 s) preceded each block, informing the participant of the upcoming condition. The task included a total of 72s of rest while a fixation crosshair was displayed, which was distributed equally in three blocks of 24s at the beginning, middle, and end of the task. Individuals with a Hit rate<25% were excluded (25). RT has also been extracted. Individuals with RT<200ms were excluded (11).

Emotional N-back task (ABCD): The emotional n-back (EN-back) task engages processes related to memory and emotion regulation (20, 27). During the task, children perform 0-back (low memory load) and 2-back (high memory load) task blocks with four types of stimuli: happy, fearful, and neutral face photographs (NimStim, http://www.macbrain.org/resources.htm) and place photographs. Data are collected during two ~5-min fMRI runs each with four 0-back and 2-back blocks. At the start of each 0-back block, children are shown a target stimulus and asked to press a button corresponding to “match” when they see an identical picture and a button corresponding to “no match” when they see a different picture. During 2-back blocks, children are asked to press match when they see a picture identical to the one, they saw two trials back. Performance is quantified as percent accuracy on 0-back and 2-back blocks. Individuals with a Hit rate<25% were excluded (25). RT has also been extracted. Individuals with RT<200ms were excluded (11).

2.3. Episodic memory tasks

Picture encoding and retrieval task (LIBD and UNIBA1): The PEAR task (28) included blocks of incidental encoding and retrieval of neutral and aversive images selected from the International Affective Picture System (IAPS) (29). During the encoding run, four blocks of neutral scenes (six scenes for 3s) and four blocks of aversive scenes were continuously presented, alternating with nine blocks of rest (18s of fixation). The order of the presentation of blocks (neutral and aversive) was counterbalanced across individuals. To make the encoding incidental, participants were not informed about the subsequent recognition/retrieval phase before scanning and thus were not aware that they were engaged in a memory task. During the encoding session, participants determined whether each picture represented an ‘indoor’ or ‘outdoor’ scene and responded via a button press (left button for ‘indoor’ and right button for ‘outdoor’). The presentation order of ‘indoor’ and ‘outdoor’ scenes was randomized. A subsequent retrieval session started ~2 min after the encoding session. During retrieval, participants determined whether the scene presented was seen during the encoding session and responded via a button press (left button for ‘new’ and right button for ‘old’). The presentation order of ‘new’ and ‘old’ scenes was also randomized. During retrieval, half of the scenes were old (i.e., presented during encoding), and half were new (i.e., not presented during encoding). As with the encoding session, there were eight blocks (four neutral and four aversive) interleaved with nine rest blocks during retrieval, and the order of neutral and aversive blocks was counterbalanced across participants. We limited our

analyses to neutral scenes to exclude the confounding effect of emotion-related activation and to make findings comparable across different episodic memory paradigms acquired for the other cohorts. We classified performance based on responses during the retrieval sessions. We extracted the Hit count, reflecting the successful recognition during the retrieval of pictures studied during encoding. Individuals with a Hit rate<60% were excluded (13). RT has also been extracted.

Relational and Item Specific Encoding task (UNIBA2)*:* During the RISE, participants performed two runs of a novel episodic memory task adapted from a previously published paradigm (12, 30). A total of 140 nameable color photographs were drawn from the FRIDa dataset (31). All pictures depicted common objects without texts and symbols, placed on a white background, and resized to a standard size of 530×530 pixels. Stimuli were presented in pairs during both encoding and retrieval conditions. Participants completed one encoding and one retrieval run. During encoding, participants studied the association between picture pairs. Pictures forming a pair were presented simultaneously on the screen for 2000 ms with a 1.5- to 2.5-second jittered intertrial interval, one on the left and one on the right. Participants completed 35 relational encoding trials (e.g., 'Can one object fit inside the other?'), responding with two separate button pads ('left' and 'right' response). During retrieval trials, participants were presented with 70 picture pairs, of which 35 were studied in the same configuration during encoding trials (unchanged), and 35 were rearranged compared to the encoding trials (changed). We compared valence, familiarity, typicality, complexity, brightness, spatial frequency, and size through an independent sample t-test, pairing each set of unchanged and changed pictures (Table S5). Participants made a 2-button response to indicate whether object pairs were unchanged ('left') or changed ('right'). Interleaved with both encoding and retrieval trials, participants were presented with pairs of scrambled pictures also for 2000 ms (10 pairs during encoding and 20 pairs during retrieval). Scrambled images forming a pair were half the time both resized to a standard size of 530×530 pixels, while the other half of the time, one was upsized and the other downsized by 30%, to preserve identical screen brightness. This condition was designed to reset the BOLD signal in the medial temporal lobe to baseline, enhancing task-related activity (32). To match motor demands of encoding and retrieval trials, participants performed a proxy of encoding trials (e.g., 'Can one scrambled picture fit inside the other?'), responding with two separate button pads ('left' and 'right' response). Participants completed a practice version of the encoding and retrieval tasks before scanning. We classified performance based on responses during the retrieval sessions. We extracted the Hit count, reflecting the successful recognition during the retrieval of pictures studied during encoding. Individuals with a Hit rate<60% were excluded (30). RT has also been extracted.

2.4. Emotion recognition tasks

Picture and Face Matching task (LIBD and UKB): During the FMT (15), participants were asked to match one of two simultaneously presented images with an identical target image. As a sensorimotor control task, the subjects were asked to match geometric shapes. The fMRI paradigm consisted of nine experimental blocks: two blocks each of matching facial expressions and matching emotionally charged visual complex pictures from IAPS (29) interleaved with five control blocks, each lasting 32 s for a total scan length of 4.48 min. Each block began with a brief (2 s) instruction statement: 'match faces', 'match Pictures', or 'match Forms'. Each matching block consisted of six images. For each face block, three images of each gender and target affect (angry or afraid) were presented. For each IAPS block, three images of each threat origin (natural or artificial) were presented. For each control block, six different geometric shapes were presented as targets. All images were presented sequentially, with no interstimulus interval, for a period of 5 s and in a randomized fashion for all conditions. The order of the paradigm was counterbalanced

across subjects. For facial expressions, 12 different images were used, 6 of each gender and affect (angry or afraid), all derived from a standard set of pictures of facial affect (33). For IAPS stimuli, 12 different images were also used, 6 representing threats of natural origin (i.e., dogs, sharks, snakes, spiders) and 6 threats of artificial origin (i.e., guns, car accidents, plane crashes, explosions). None of the IAPS images contained human faces. The mean valence and arousal on a nine-point scale, where one represents maximum negative and nine maximum positive valences or arousals, for all IAPS stimuli used were 3.13 ± 0.20 and 6.40 ± 0.13, respectively. Simple geometric shapes (circles, vertical, and horizontal ellipses) were used as control stimuli.

Faces task (UNIBA1): The Faces (17, 34) acquired for the UNIBA1 dataset consisted of one event-related run, presenting angry, fearful, happy, and neutral facial expressions from a validated set of facial pictures (NimStim, http://www.macbrain.org/resources.htm). The order of stimuli was randomly distributed. During the execution of the task, emotional perceptual processing (implicit processing), participants identified the gender of each face. From stimulus appearance, two seconds were allowed for behavioral responses. Each stimulus was presented for 500 ms, with the interstimulus interval randomly jittered between 2 and 7 seconds. The total number of stimuli was 144 of which 30 were angry, 39 fearful, 37 happy, and 38 neutral faces. A fixation crosshair was presented during the interstimulus interval. The duration of the entire run was 6 minutes and 8 seconds.

Faces task – revised version (UNIBA2): During the implicit emotion recognition session, participants performed a revised version of the Faces task (16, 35) previously described in section 2.3.5. This task consists of a presentation of angry, fearful, and neutral facial expressions from the FACES database (36). Stimuli order was pseudorandom. From stimulus appearance, 2 s were allowed for behavioral responses. Each stimulus was presented for 500 ms, with a response deadline of 2000 ms from the onset. The interstimulus interval pseudo-randomly jittered between 2 and 7 s (inter-stimulus-interval average after jittering: 2.7 s). The total number of stimuli was 108 of which 36 were angry, 36 fearful, and 36 neutral faces. A fixation crosshair was presented during the interstimulus interval. Subjects indicated whether the face presented was ‘male’ or ‘female’.

Emotion identification task - Emo (PNC): the Emo task (19) employs a fast event-related design with a jittered inter-stimulus interval (ISI). Subjects viewed 60 faces displaying neutral, happy, sad, angry, or fearful expressions, and were asked to label the emotion displayed. Briefly, the stimuli were color photographs of actors (50% female) who volunteered to participate in a study on emotion. Actors were coached by professional directors to express a range of facial expressions. For the present task, a subset of intense expressions was selected based on a high degree of accurate identification (80%) by raters. Each face was displayed for 5.5 seconds followed by a variable ISI of 0.5 to 18.5 seconds, during which a complex crosshair (that matched the faces’ perceptual qualities) was displayed.

3. Behavioral analysis

To assess behavioral differences in terms of working memory and episodic memory performance, we compared the accuracy and performance speed in terms of RT through Welch two-sample t test between:

- yNC vs oNC to test for age-related differences in cognitive abilities.
- yNC vs ySIB (LIBD) to test for familial risk-related differences in cognitive abilities during late adolescence and early adulthood.

- aNC vs oSIB (LIBD) to test for familial risk-related differences during later adulthood.
- ySIB vs oSIB (LIBD) to test whether familial risk-related differences in cognitive abilities varied by age group.
- cNC vs cSIB/FHR (PNC and ABCD) to test for familial risk-related differences in cognitive abilities during childhood.
- cNC vs cPSY (PNC and ABCD) to test for clinical risk-related differences in cognitive abilities during childhood.
- yNC vs yPSY (UNIBA2 and PNC) to test for clinical risk-related differences in cognitive abilities during late adolescence and early adulthood.

Statistical significance was set at $p<0.05$. Behavioral performance collected during working and episodic memory tasks is shown in Table S3. Results showing differences across age-related and risk-related groups are shown in Figure S2.

4. **Acquisition and processing of MRI data**

Structural and functional scans acquired for the six cohorts are described in Table S4. Notably, in the UNIBA2 cohort resting state has been acquired using two different sequences. We accounted for this difference in the following group-level analysis, specifying repetition time (TR) and the number of volumes as covariates (37). In the ABCD cohort, four resting state acquisitions for each individual were available. We took into account data of individuals who completed at least two of the fMRI sessions included in the experimental protocol. The MRI data underwent an individual Quality Check (QC) pipeline to retain only data that were not affected by any technical artifact. Specifically, all raw fMRI images from each session, as well as the T1-weighted structural image, were examined via visual inspection to detect artifacts like blurring, ringing, wrapping (38, 39) and excessive noise, poor image contrast and/or poor boundaries (38, 40). Regarding head coverage, T1 images were excluded in case of cropping. The crop of dorsal and frontal regions was also checked for fMRI images.

LIBD, UNIBA1, UNIBA2. Individual raw structural images were reoriented with the origin in the anterior commissure and the axial plane aligned along the anterior and posterior commissure axis (AC-PC line). Individual structural images were pre-processed with Statistical Parametric Mapping (SPM) version 12 (http://www.fil.ion.ucl.ac.uk/spm) and the Computational Anatomy Toolbox (CAT12, http://dbm.neuro.uni-jena.de/cat/), under the MATLAB 2019b environment. 3D MPRAGE T1-weighted segmentation served to estimate grey matter (GM), white matter (WM), and cerebrospinal fluid (CSF) (41). Bias correction removed intensity non-uniformities. Whole brain images acquired for each fMRI acquisition covered the entire cerebrum and most of the cerebellum was acquired for each participant. All functional images were individually examined and carefully screened for data quality using visual inspection for image artifacts, estimating indices for ghosting artifacts, and signal-to-noise ratio across the time series. Images were reoriented to the anterior commissure-posterior commissure (AC-PC) line with the origin in the AC. Then, images were realigned to the mean image of the scan run, co-registered to the individual anatomical image and unwarped, spatially normalized to a $3 \times 3 \times 3$ mm^3 voxel size into a standard stereotactic space using affine and non-linear transformation through the Symmetric Normalization function implemented in the Advance Normalization toolbox – ANTs (42), and smoothed using a 9-mm full-width at half-maximum isotropic 3D Gaussian kernel. fMRI scans were normalized to the standard Montreal Neurological Institute (MNI) space. Concerning head motion correction, functional images were inspected to check for excessive motion correction (>3 mm in translation and >1.5 degrees

in rotation). We also computed ensured that the movement of the head from one frame to the next during acquisition, measured through FD, was lower than the published threshold (FD<0.05) (43). Additionally, twenty-four motion parameters (44) were regressed to limit the effect of motion on connectivity estimates.

PNC. Individual raw structural images were reoriented with the origin in the anterior commissure and the axial plane aligned along the anterior and posterior commissure axis (AC-PC line). Individual structural images were pre-processed with SPM12 and the CAT12 Toolbox, under the MATLAB 2019b environment. 3D MPRAGE T1-weighted segmentation served to estimate grey matter (GM), white matter (WM), and cerebrospinal fluid (CSF) (41). Bias correction removed intensity non-uniformities. Due to the rapid development of the brain, brain reference templates for children have been suggested for MRI investigations in neurodevelopmental cohorts (45-48) to reduce the requirement for spatial deformation during image normalization and maintain a great number of developmental characteristics of individual brains (46). Furthermore, morphological differences have been reported in the neurodevelopmental cohort between males and females (49-51). For normalization purposes, we built customized templates for individuals from 8 to 14 years of age included in the PNC sample. Specifically, we calculated two separate 8-14-years-old customized templates, one for the female sample, and one for the male sample, to minimize registration bias and maximize sensitivity to detect regional effects that can be impacted by registration errors. We randomly selected data from 50 females and 50 males from the PNC sample considering a 3:2 ratio across groups, i.e., cNC vs cPSY. We use the Multivariate Template Construction function implemented in ANTs (52). We run repeatedly the algorithm for seven concatenated iterations (45). During the preliminary iteration (zero), each structural image was co-registered, and a temporary shared-space template is computed. During the following iterations, all the individual structural images were (i) registered to the temporary shared-space template that had been generated one iteration before, (ii) then co-registered, and (iii) a new shared-space template is computed. We used a linear rigid registration through the Symmetric Normalization (SyN) transformation model (52) that maximizes the cross-correlation within the space of diffeomorphic maps across individuals. Whole brain images acquired for each fMRI acquisition covered the entire cerebrum and most of the cerebellum was acquired for each participant. All functional images were individually examined and carefully screened for data quality using visual inspection for image artifacts, estimating indices for ghosting artifacts, and signal-to-noise ratio across the time series. Images were reoriented to the anterior commissure-posterior commissure (AC-PC) line with the origin in the AC. Then, images were realigned to the mean image of the scan run, co-registered to the individual anatomical image and unwarped, spatially normalized to a 3 × 3 × 3 mm^3 voxel size into a standard stereotactic space using affine and non-linear transformation through the Symmetric Normalization function implemented in ANTs (42), and smoothed using a 9-mm full-width at half-maximum isotropic 3D Gaussian kernel. fMRI scans of individuals ≥15 years old were normalized to the standard MNI template space, while fMRI scans of individuals <15 years old were normalized to age- and sex-customed templates' space previously described in this paragraph. Concerning head motion correction, functional images were inspected to check for excessive motion correction (>3 mm in translation and >1.5 degrees in rotation). We also computed ensured that the movement of the head from one frame to the next during acquisition, measured through FD, was lower than the published threshold (FD<0.05) (43). Additionally, twenty-four motion parameters (44) were regressed to limit the effect of motion on connectivity estimates.

ABCD. We downloaded the ABCD FastTrack images with recommended active series from NDA. The FastTrack images are unprocessed imaging data that completed and passed raw quality control (QC). We preprocessed the raw fMRI data using a combination of FMRIB Software Library v6.0 (FSL) toolbox and SPM12 toolbox, under the MATLAB 2019b environment. Rigid body motion

correction was performed using the *mcflirt* tool in FSL before the distortion correction. The ABCD fMRI field map data were collected with the phase-reversed blips, producing pairs of images with distortion occurring in opposite directions. Volumes acquired with phase encoding in the anterior-posterior (AP) direction and volumes with phase encoding in the posterior-anterior (PA) direction were used with the FSL tool *top-up* to estimate the susceptibility-induced off-resonance field. The output field map coefficients were used to correct the distortion in the fMRI volume using the FSL tool *applytopup*. After distortion correction, we discarded 10 initial scans with large signal changes to allow the tissue to reach a steady state of radiofrequency excitation. Next, the fMRI data were warped into the standard MNI space based on the echo-planar imaging (EPI) template, resampling to 3 × 3 × 3 mm^3 isotropic voxels using the normalization tool in SPM. The resliced fMRI images were subsequently smoothed using a Gaussian kernel with a 6-mm full-width at a half-maximum isotropic 3D Gaussian kernel. Concerning head motion correction, functional images were inspected to check for excessive motion correction (>3 mm in translation and >1.5 degrees in rotation). We also computed ensured that the movement of the head from one frame to the next during acquisition, measured through FD, was lower than the published threshold (FD<0.05) (43). As ABCD data have been acquired by 29 different MRI scanners across 21 sites, the scanner was used as a regression to limit its effect on connectivity estimates. Participants who did not show good normalization of their fMRI images to the MNI standard space were excluded from further analysis. Specifically, we compared individual masks with the group mask and retained those individuals with a high similarity between the individual masks and the group mask. First, based on the first fMRI time volume, we calculated the individual mask for each subject by setting voxels to 1 if they are greater than 90% of the whole brain mean. Next, we computed a group mask by setting voxels to 1 if they have more than 90% of the subjects with 1 for individual masks. For each subject, we then calculated the spatial correlations between the group mask and the individual mask. The spatial correlations were calculated using voxels within the top 10 slices of the mask, within the bottom 10 slices of the mask, and of the whole mask, resulting in three correlations for each subject. If a subject has a top-10-slices correlation larger than 0.75, a bottom-10-slices correlation larger than 0.55, and a whole-brain correlation larger than 0.8, we include this subject for further analysis. This method can ensure we have a high-quality mask and fMRI data for all individuals.

UKB. Full details of the image acquisition and processing can be found on the UKB website (http://biobank.ctsu.ox.ac.uk/crystal/refer.cgi?id=2367), Brain Imaging Documentation (http://biobank.ctsu.ox.ac.uk/crystal/refer.cgi?id=1977). Our study made use of pre-processed image data generated by an image-processing pipeline developed and run on behalf of UKB by Alfaro-Almagro*, et al.* (53). Specifically, MRI data for all participants were acquired on the same Siemens Skyra 3T scanner (Cheadle, Manchester site). Briefly, the acquired 3D MPRAGE T1-weighted and EPI volumes were pre-processed and analyzed using FSL by the UKB brain imaging team. No significant changes were made to scanner hardware or software during the period of MRI data acquisition; full details on protocol phases and relevant upgrades are publicly available (http://biobank.ctsu.ox.ac.uk/crystal/docs/brain_mri.pdf). The following processing was applied to the EPI volumes: motion correction using *mcflirt*, grand-mean intensity normalization of the entire 4D dataset by a single multiplicative factor; high pass temporal filtering (Gaussian-weighted least-squares straight line fitting, with sigma=50.0s); EPI unwarping combined with the alignment to the T1, though the unwarped data is written out in native (unwarped) fMRI space (and the transform to T1 space written out separately). The data is nonlinearly warped to MNI space using *fnirt* (FMRIB's Nonlinear Image Registration Tool. Spatial smoothing (using a Gaussian kernel of 6 mm full-width) was applied. Quality checks of EPI volumes were initially carried out by UKB with further local quality control procedures. Individual EPI volumes were visually checked and removed case-wise in instances of aberrant normalization or artifacts.

Neuromark pipeline. To estimate individual-level brain FNC features, we used the Neuromark pipeline (54) on multiple fMRI scans including resting state, working memory, episodic memory, and emotion recognition tasks in all cohorts. We used multi-objective optimization ICA with reference (MOO-ICAR) algorithm (55) available in the group ICA of fMRI toolbox (GIFT) (http://trendscenter.org/software/), by taking each participant's fMRI data as input. We used 53 labeled and ordered IC templates arranged into seven functional domains (e.g., auditory [AU, N = 2], cerebellar [CB, N = 4], cognitive control [CC, N = 17], default mode [DM, N = 7], sensorimotor [SM, N = 9], sub-cortical [SC, N = 5], visual [VI, N = 9]) as the spatial priors for guidance in estimating subject-specific networks (54).

We obtained whole-brain FNC estimates by computing Pearson's correlations between the time courses of each IC to yield an FNC matrix reflecting the relationship between any two IC for each fMRI session. In this FNC matrix, higher values correspond to higher connectivity between two IC time courses, whereas lower values correspond to lower connectivity between two IC time courses. We considered a spatial overlap of>75% between each IC spatial map and the whole-brain fMRI acquisition at the individual level to exclude the ICs that were not included in the individual fMRI image acquisition (56, 57).

5. Participants' genotype determination and Polygenic-Risk Score calculation

For LIBD, UNIBA1, and UNIBA2 participants underwent blood withdrawal for subsequent DNA extraction from peripheral blood mononuclear cells. To this aim, approximately 20ml of fresh blood was obtained through a conventional venous blood collection with 10ml EDTA Vacutainer Venous Blood Collection Glass Tubes (Vacutainer ®). Approximately 200 ng of DNA was used for genotyping analysis. DNA was concentrated at 50ng/µl (diluted in 10 mM Tris/1 mM EDTA) with a Nanodrop Spectrophotometer (ND-1000). Samples were genotyped using variate Illumina Bead Chips including 510K/610K/660K/2.5M. For PNC, Genome-wide genotyping in PNC has been performed in waves using six different genotyping platforms. Genotypes are available through the NIMH Database of Genotypes and Phenotypes (dbGaP; https://www.ncbi.nlm.nih.gov/projects/gap/cgi-bin/study.cgi?study_id=phs000607.v3.p2). For ABCD, genotyping was performed with the Smokescreen™ Genotyping array (58). Genome-wide genotyping was performed on all UK Biobank participants using the UK Biobank Axiom Array. Approximately 850,000 variants were directly measured, with > 90 million variants imputed using the Haplotype Reference Consortium and UK10K + 1000 Genomes reference panels.

Quality control was performed on the cohorts separately using PLINK (version 1.07; http://pngu.mgh.harvard.edu/purcell/plink/) (59) according to standards developed by the Psychiatric Genomics Consortium [PGC (60, 61)] including SNP missingness < 0.05 (before sample removal); subject missingness < 0.02; autosomal heterozygosity deviation (|Fhet| < 0.2); SNP missingness < 0.02 (after sample removal), SNP Hardy-Weinberg equilibrium (HWE: P > 10−6) and minor allele frequency (MAF) > 0.01. Furthermore, the degree of recent shared ancestry, i.e., the identity by descendent (IDB) (62), has been estimated within the cohorts to define the relatedness of all pairs on individuals through the PLINK function '--genome' (63). The threshold 0.125 represents the relatedness of 3rd degree (64) that was used as a cut-off to exclude the possible influence of relatedness within cohorts on the dependency between observations (65). Of each pair of related individuals, the one belonging to the group with greater numerosity within each cohort is dropped from the final datasets. Only Caucasian individuals have been included in the analysis. Characteristics of individuals included in the genetic analysis grouped by cohort are reported in Table S6.

Genotype imputation was performed using the pre-phasing/imputation stepwise approach implemented in IMPUTE2 / SHAPEIT (chunk size of 3 Mb and default parameters) and using Phase 3 1000 genome as a reference panel (66, 67). After imputation, imputed dosage data for each SNP with imputation quality (INFO) > 0.9 were used for polygenic risk scores (PRS) calculation.

To study the genetics underlying the deviating FNC patterns, we analyzed the relationship between averaged FNC patterns across multiple fMRI acquisitions and PRS constructed based on risk loci from the most recent schizophrenia GWAS SNPs [PGC3 GWAS (60, 61)]. For the LIBD cohort, SNPs in linkage equilibrium (R^2<0.1) that span across the whole genome were used. We then computed a weighted sum of risk alleles for schizophrenia, by summing the imputation probability for the reference allele of the index SNP, weighted by the natural log of the odds ratio of association with schizophrenia, at each independent locus across the whole genome, as described elsewhere (68). For all the other cohorts we followed the same PRS calculation illustrated before through the PRSice-2 toolbox (69).

Consistent with the original approach taken in the Schizophrenia Working Group of the Psychiatric Genomics (61) GWAS study, ten PRSs (PRS1–10) were calculated using subsets of SNPs selected according to the GWAS p-value thresholds of association with schizophrenia: 5×10^{-08} (PRS1), 1×10^{-06} (PRS2), 1×10^{-04} (PRS3), 0.001 (PRS4), 0.01 (PRS5), 0.05 (PRS6), 0.1 (PRS7), 0.2 (PRS8), 0.5 (PRS9), and 1 (PRS10). SNPs in sets with lower p-values are also in sets with higher p-values (for example, SNPs in PRS1 are included in PRS2, SNPs in PRS2 are included in PRS3, and so on).

To control for population stratification in the association analysis, the first 10 principal components of the whole genome data were calculated using EIGENSOFT v5.01 (EIGENSOFT, http://www.hsph.harvard.edu/alkes-price/software/) and considered as nuisance covariates in genetic analysis.

6. Control analysis

6.1 FNC differences during each fMRI session

We considered the age-group × session interaction, as described in the main text, Sections 2.2 and 4.4, included in the linear mixed effect models for each IC pair to assess whether FNC differences between yNC and oNC are dependent on a single fMRI session. There were no significant age-groups by session interactions in any of the 17 age-related IC pairs where we identified age differences across all sessions. We additionally examined the remaining 1353 IC pairs for completeness, discovering a consensus across cohorts on three IC pairs (empirical p-value of such a high consensus across cohorts 3×10^{-4}).

A total of 384 IC pairs showed a significant difference between yNC and oNC in the LIBD cohort, a total of 535 IC pairs showed a significant difference between yNC and oNC in UNIBA1, and a total of 190 IC pairs showed a significant difference between yNC and oNC in UNIBA2. We found a consensus across the LIBD, UNIBA1, and UNIBA2 cohorts on three IC pairs included in the CC (N = 1), SC (N = 1), CB (N = 1), VI (N = 2), non-overlapping with the IC pairs in which we found age differences considering all sessions. Results are depicted in Figure S4.

In the three IC pairs in which we found an age-groups × session interaction, no significant differences emerged when comparing yNC vs ySIB and oNC vs oSIB. Instead, we found a significant diagnosis effect (oNC vs oSCZ and oSIB vs oSCZ) within the visual network, in which oSCZ showed lower FNC as compared with oNC and oSIB during working memory (respectively, pFDR = 1.37×10^{-12} and pFDR = 4.21×10^{-7}), and significant differences between oNC and oSCZ in the cerebellar-thalamic circuit during the encoding and retrieval of the episodic memory task (respectively, pFDR = 1.2×10^{-8} and pFDR = 1.74×10^{-4}).

Further, we analyzed the relationship between PRS and FNC for each fMRI session with the mixed-effect meta-analytic procedure (See the main text, Section 4.6). We found no significant association between FNC and PRS (pFDR>0.05), although the direction remained the same as in averaged results in the cerebellar-occipitoparietal FNC × PRS association during the encoding and the retrieval of the episodic memory task (respectively, r=-0.13 and r=-0.09), resting state (r=-0.06), and the emotion recognition task (r=-0.02). Also, the direction of the medial PFC-occipitoparietal FNC × PRS association during the encoding and the retrieval of the episodic memory task with PRS (respectively, r=0.06 and r=0.08) during the working memory (r=0.12), and the emotion recognition task (r=0.05), resulted in the same direction of the averaged FNC × PRS results. Similarly, the direction of the dorsolateral PFC-occipitoparietal FNC × PRS association during the encoding and the retrieval of the episodic memory task with PRS (respectively, r=0.01 and r=0.07), during the working memory (r=0.15), and the emotion recognition task (r=0.04), resulted in the same direction as the averaged FNC × PRS results. Further confirming that risk was unrelated to changes in connectivity across sessions, no significant FNC × PRS associations emerged in the three IC pairs in which we found an age-groups × session interaction. Results are depicted in Figures S5 and S6.

6.2 Association between PRS and FNC in children

In PNC and ABCD cohorts, we found no significant FNC differences comparing cNC vs cSIB/FHR, as well as cNC vs cPSY (see the main text, Section 2.4 and Figure S7), confirming the hypothesis that risk-related FNC patterns emerge only during adolescence and early adulthood but not before, in line with the neurodevelopmental hypothesis (70). We hypothesized that since children do not show risk-related alterations in FNC patterns, the latency of these brain patterns would not be detectable by polygenic risk as measured by PRS in neurotypical individuals, individuals at familial risk for schizophrenia, or individuals with subthreshold psychotic symptoms. Thus, we examined the FNC × PRS association in children from PNC and ABCD using the same approach outlined in section 4.6 of the manuscript. We found no significant association (pFDR>0.05; Figure S8), further strengthening our interpretation for these risk-related FNC patterns are transient and emerge not before adolescence. Also, the fact that individuals may show psychotic manifestations during childhood, but rarely a full-blown psychosis during this age-stage, may be related to this mechanism of latency of risk-related brain characteristics.

6.3 Age by PRS interaction

To test whether the effect of PRS on FNC varies at different age-stages, we extracted from the meta-analytic model across cohorts as described in the manuscript in Section 4.6. We found a significant age-group × PRS interaction in the cerebellar-occipitoparietal circuit and in the dorsolateral-PFC circuit (Figure S9d,f; pFDR<0.05). More specifically, we found that younger individuals show a larger effect as compared with older individuals in the cerebellar-occipitoparietal circuit (Figure S9g). In the dorsolateral PFC circuit, the interaction seems to be driven by the UNIBA1 site with a strong association between FNC and PRS3, not significant in the older group (Figure S9h); on the other hand, the interaction patterns of FNC with PRS4 appear to be more consistent over cohorts, with no significant main effects in either group (Figure S9i). Notably, the interactions in the dorsolateral PFC-sensorimotor circuit were identified with PRS3 and 4, the main effect of which was not significant (Figure S9c). Furthermore, spitting the datasets necessarily reduces statistical power, thus smaller and more unstable effects have been reported within age-groups for each cohort, compared to the magnitude of the overall main effects identified (Figure S9d-e). Therefore, these results possibly suggest a larger effect size at younger ages, further

supporting the hypothesis of risk patterns depletion in older individuals in the cerebellar-occipitoparietal and the dorsolateral PFC-sensorimotor circuits, but the interactions appear less consistent than the main effects. Interestingly, no age-group × PRS interaction has been found in the medial PFC-sensorimotor circuit where the risk patterns persisted in older individuals (Figure S9e).

6.4 Group differences in GM estimates matching FNC patterns

To determine whether FNC alterations in oSCZ are caused by structural changes, we analyzed brain structural differences in terms of voxel-wise individual grey matter (GM) estimates across age-stages following the same pipeline of the FNC analyses. We processed individual T1-weighted structural scans through the Computational Anatomy Toolbox (CAT12, http://dbm.neuro.uni-jena.de/cat/) as described in SI Appendix, section 4. We extracted individual estimates of GM from each brain region included in the 53 Neuromark IC to match the functional IC and make functional and structural metrics comparable.

First, we assessed age-stage differences between yNC and oNC in the LIBD, UNIBA1, and UNIBA2 cohorts. Familial risk-related structural patterns were tested by comparing yNC vs ySIB, and oNC vs oSIB. Clinical risk-related structural patterns were assessed by comparing yNC and yPSY in the UNIBA1 and UNIBA2 cohorts. Finally, the investigated GM differences in oSCZ as compared with oSIB and oNC at the same age-stage. We accounted for multiple comparisons through the Benjamini-Hocberg correction using the number of IC considered (k=53). To obtain one p-value estimate for each IC pair instead than one per cohort, we then combined reproducible effects via Fisher's combined probability test using the 'metap' package implemented in R Statistics (https://cran.r-project.org/).

We found a consensus on 25 ICs comparing yNC vs oNC including the medial and dorsolateral PFC, the sensorimotor, the cerebellar, and the occipitoparietal ICs, in which we reported functional age-related differences (pFDR<0.05). No consistent significant differences across cohorts have been found comparing the risk groups, i.e., yNC vs ySIB; yNC vs yNC; oNC vs oSIB while comparing oNC vs oSCZ we found significantly reduced GM estimates in the medial PFC ($p=2.2 \times 10^{-6}$) and the sensorimotor cortex (p=0.02) overlapping with the risk-related medial PFC-sensorimotor circuit functionally determined. Also, we found reduced GM estimates in oSCZ in the anterior cingulate cortex ($p=2.6 \times 10^{-4}$), in the inferior frontal gyrus (p=0.001), and in the bilateral insula (p=0.04). As these analyses aimed to explore the structural contribution to the schizophrenia-related FNC patterns reported in the present study, we tested the relationship between medial PFC and sensorimotor GM, finding a strong association in oSCZ (r=0.89; $p=2.2 \times 10^{-16}$; Figure S10a) and in all groups (p<0.05; Figure S10b), suggesting that the reduction of GM in these two brain regions covaries.

Additionally, we tested the association between GM patterns and Chlorpromazine Equivalents across cohorts, finding a significant negative association both with the medial PFC GM (r=-0.39; p=0.0009; Figure S10c) and with the sensorimotor cortex GM (r=-0.24; p=0.011; Figure S10d), suggesting a direct inverse association of antipsychotic medication dose on GM and a potential indirect effect on FNC in these regions. Instead, no significant association has been identified between dorsolateral PFC and Chlorpromazine Equivalents, even though this region showed reduced GM in oSCZ, suggesting specificity of the treatment effect for the medial PFC-sensorimotor circuit.

To assess whether reduced GM mediates genetic effects, we tested the association between GM estimates and PRS, which was not significant (pFDR>0.05; Figure S10e). Overall, the findings are consistent with an effect of environmental variables, at least in part associated with drug administration, that may confound the FNC findings.

6.5 Cognitive differences across groups

To better characterize cognition abilities in NC, SIB, and SCZ, we examined individual performance out of the scanner in a set of neuropsychological tests widely studied in SCZ (71). In particular, we used the cognitive hierarchical factors identified by Dickinson, Goldberg, Gold, Elvevag and Weinberger (72) on the LIBD individuals also included in this study, which accounted for cognitive variables which have been shown to classify SCZ at ~80% (73). We replicated the factorial model in two subsets of participants from UNIBA1 and UNIBA2 that were administered a neuropsychological battery including the Wechsler Adult Intelligence Scale-Revised version (74), Trails Making Test (75), Wechsler Memory Scale (76), and N-Back (10) out of the MRI scanner (Table S7). PNC, UKB, and ABCD cohorts also include a neuropsychological assessment, though not overlapping with the one used in LIBD, UNIBA1, and UNIBA2, thus it has not been possible to replicate the factorial model here considered.

A Confirmatory Factorial Analysis (CFA) yielded factors for verbal memory, visual memory, processing speed, digit span, N-back performance, and card sorting, as in the original publication. Individual loadings for LIBD have been extracted from the original publication (72). Because the cognitive assessment in UNIBA1 and UNIBA2 was identical and cognitive assessment of the MRI scanner was not available for all individuals for each neuropsychological measure (30% on average), we jointly considered the two UNIBA cohorts to improve the factorial solutions of the CFA. The final sample size for each cohort is reported in Table S7. The factor solution was consistent with Dickinson, Goldberg, Gold, Elvevag and Weinberger (72), in terms of the assignments of individual cognitive variables and the magnitude of loadings (Figure 12). Consistently, performance in oSCZ significantly differed from oNC for each factor ($p<0.05$, Figure S13a-f). Moreover, using the same statistical approach that we used for FNC analysis in this study to summarize consistent results across cohorts, we found significant differences between yNC and oNC only for processing speed and carding sorting factors ($p=0.05$ and $p = 0.04$). When analyzing SIB groups, risk differences were significant comparing oNC and oSIB in verbal memory and N-back performance ($p=0.01$ and $p = 0.02$; Figure S13b,d). Furthermore, verbal memory performance resulted negatively associated with FNC in the medial and dorsolateral PFC-sensorimotor circuits in ySIB and oSCZ ($p<0.05$, Figure S13), but not in oSIB, as well as in oNC, further supporting our interpretation of a more pronounced risk effect in SIB associated with the emergence of risk-related FNC pattern during adolescence and early adulthood. However, given the variable availability of data across the cognitive variables considered within each cohort, and given that some groups are not even represented, we think additional investigations in larger cohorts are necessary to establish the relationship between cognition and FNC.

6.6 FNC variability across groups

We hypothesized that SCZ might show higher variability than SIB and NC at the same age-stage due to the high heterogeneity of SCZ manifestations. This hypothesis is sustained by recent investigations on interindividual variability of functional brain features that reported higher variability in terms of brain activity and connectivity in patients with schizophrenia (77, 78). We compared the variance of FNC across groups through the Fligner-Killeen test, a non-parametric test for homogeneity of group variances based on ranks. We found that oSCZ showed significantly higher variance in the cerebellar-occipitoparietal and dorsolateral PFC-sensorimotor circuits compared to oNC (respectively, $\chi^2 = 6.68$; $p = 0.009$; $\chi^2 = 95.53$; $p = 2.2 \times 10^{-16}$), and oSIB (respectively, χ^2

= 6.2; p = 0.002, χ^2 = 9.30; p = 0.001). These results suggest that the higher variability in oSCZ might have impacted the significance of group differences diluting the effects (79).

SI Tables

Table S1. Description of the sample size available for each fMRI session.

Cohort	Group [N]	Resting state N	N-Back/ EN-Back N	PEAR/RISE encoding N	PEAR/RISE retrieval N	FMT/Faces/Emo N
LIBD	yNC [200]	121	167	123	131	143
	oNC [246]	122	197	148	146	166
	ySIB [41]	19	25	15	16	20
	oSIB [40]	22	35	22	20	23
	oSCZ [88]	34	66	42	45	50
UNIBA1	yNC [356]	138	317	66	50	148
	oNC [125]	58	112	18	14	53
	ySIB [12]	0	12	5	0	8
	oSIB [46]	0	42	19	0	18
	oSCZ [82]	0	47	42	26	16
UNIBA2	yNC [127]	93	80	58	54	73
	oNC [57]	46	44	36	35	20
	yPSY [46]	32	30	18	20	21
	oSCZ [25]	12	16	7	5	11
PNC	cNC [90]	75	56	0	0	49
	yNC [74]	68	59	0	0	52
	cPSY [44]	34	30	0	0	25
	yPSY[79]	68	71	0	0	64
ABCD	cNC [3636]	3636	112	0	0	0
	cSIB/FHR [62]	62	3	0	0	0
	cPSY [1238]	1238	43	0	0	0
UKB	oNC [2520]	2520	0	0	0	2520

Table S2 Site-per-site description of the neuropsychological task acquired for each cognitive domain. Abbreviations: PEAR = Picture encoding and retrieval; RISE = relational and item-specific encoding; FMT = Faces matching task.

Cognitive domains	LIBD	UNIBA 1	UNIBA 2	PNC	ABCD	UKB
Working memory	N-Back (10)	N-Back (10)	N-Back (10)	N-Back (18)	EN-Back (20, 21)	/
Episodic Memory	PEAR (13)	PEAR (13)	RISE (12)	/	/	/
Emotion recognition	FMT (35)	Faces (34)	Faces Revised (34)	Emo (19)	/	FMT (35)

Table S3 Behavioral performance during the working memory and the episodic memory tasks across cohorts, i.e., LIBD, UNIBA1, UNIBA2, PNC, ABCD.

Cohort	Group	Working memory		Episodic memory	
		Mean Hit Rate ± SD (%)	Mean Reaction Times ± SD (seconds)	Mean Hit Rate ± SD (%)	Mean Reaction Times ± SD (seconds)
LIBD	yNC	83.65 ± 15	0.398 ± 0.18	90.09 ± 7	1.149 ± 0.17
	oNC	77.35 ± 16	0.508 ± 0.26	87.37 ± 9	1.207 ± 0.17
	ySIB	79.12 ± 17	0.496 ± 0.24	88.14 ± 8	1.106 ± 0.14
	oSIB	71.08 ± 16	0.599 ± 0.29	88.41 ± 7	1.255 ± 0.17
	oSCZ	72.09 ± 18	0.602 ± 0.19	84.51 ± 9	1.323 ± 0.16
UNIBA1	yNC	82.07 ± 17	0.523 ± 234	92.61 ± 7	1.098 ± 0.18
	oNC	80.28 ± 17	0.620 ± 235	91.05 ± 7	1.162 ± 0.19
	oSIB	66.01 ± 21	0.721 ± 0.257	93.76 ± 5	1.169 ± 0.23
	oSCZ	59.14 ± 18	0.763 ± 0.194	89.20 ± 9	1.401 ± 0.35
UNIBA2	yNC	78.18 ± 14	0.403 ± 0.27	80.08 ± 9	1.078 ± 0.09
	oNC	71.40 ± 18	0.496 ± 0.22	80.80 ± 8	1.095 ± 0.11
	yPSY	74.11 ± 20	0.535 ± 0.24	80.25 ± 7	1.142 ± 0.09
	oSCZ	53.81 ± 15	0.831 ± 0.26	76.37 ± 7	1.168 ± 0.06
PNC	cNC	77.45 ± 17	0.627 ± 0.18	/	/
	cPSY	86.25 ± 13	0.544 ± 0.11	/	/
	yNC	89.42 ± 13	0.561 ± 0.12	/	/
	yPSY	82.36 ± 14	0.512 ± 0.11	/	/
ABCD	cNC	76.19 ± 13	1.005 ± 0.12	/	/

	cSIB/FHR	80.04 ± 9	0.890 ± 0.19	/	/
	cPSY	67.57 ± 18	1.022 ± 0.14	/	/

Table S4. Site-per-site description of the structural MRI (sMRI) and the functional MRI (fMRI) sequences.

Cohort	Scanner	Sequence TYPE	TR/TE	Volumes	Voxel size (mm)	FOV (mm)/slices
LIBD	GE Signa 3T	sMRI: T1		1	1x1x1.3	256/124
		Rest fMRI: GE-EPI	2000/30	300	4x4x5	240/26
		N-back fMRI: GE-EPI	2000/30	120	3.75x3.75x5	240/26
		PEAR fMRI: GE-EPI	2000/30	85 + 85	3.75x3.75x5	240/26
		FMT fMRI: GE-EPI	2000/30	144	3.75x3.75x5	240/26
UNIBA1	GE Signa 3T	sMRI: T1		1	1x1x1.3	256/124
		Rest fMRI: GE-EPI	2000/30	150	3.75x3.75x5	240/26
		N-back fMRI: GE-EPI	2000/30	120	3.75x3.75x5	240/26
		PEAR fMRI: GE-EPI	2000/30	85 + 85	3.75x3.75x5	240/26
		Faces fMRI: GE-EPI	2000/30	180	3.75x3.75x5	240/26
UNIBA2	Philips Ingenia 3T	sMRI: T1		1	1x1x1	256/180
		Rest fMRI: EPI	2000/36	200	3x3x3	240/26
		Rest fMRI: EPI	3000/38	240	3x3x3.6	240/38
		N-back fMRI: EPI	3000/38	120	3x3x3.6	240/38
		RISE fMRI: EPI	3000/38	117 + 212	3x3x3.6	240/38
		Faces Rev. fMRI: EPI	3000/38	212	3x3x3.6	240/38
PNC		sMRI: T1		1	1x1x1	180/240

	Siemens MAGNETOM Trio 3T	Rest fMRI: EPI	3000/32	120	3x3x3	192/192
		N-Back fMRI: EPI	3000/32	231	3x3x3	192/192
		Emo fMRI: EPI	3000/32	210	3x3x3	192/192
ABCD	Siemens MAGNETOM Prisma/Prisma ^{Fit} 3T	sMRI: T1		1	1x1x1	256/176
		Rest fMRI: EPI	800/30	60 + 60 + 60 +60	2.4x2.4x2.4	216/60
		EN-Back fMRI: EPI	800/30	362	2.4x2.4x2.4	216/60
	Philips Achieva dStream/Ingenia 3T	sMRI: T1		1	1x1x1	256/225
		Rest fMRI: EPI	800/30	60 + 60 + 60 + 60	2.4x2.4x2.4	216/60
		EN-Back fMRI: EPI	800/30	362	2.4x2.4x2.4	216/60
	GE Discovery 3T	sMRI: T1		1	1x1x1	256/208
		Rest fMRI: GE-EPI	800/30	60 + 60 + 60 + 60	2.4x2.4x2.4	216/60
		EN-Back fMRI: GE-EPI	800/30	362	2.4x2.4x2.4	216/60
UKB	SIEMENS MAGNETOM Skyra 3T	sMRI: T1		1	1x1x1	256/208
		Rest fMRI: EPI	735/39	490	2.4x2.4x2.4	210/54
		FMT fMRI: EPI	735/39	332	2.4x2.4x2.4	210/54

Table S5. Independent sample t-tests comparing valence, familiarity, typicality, complexity, brightness, spatial frequency, and size across each set of matching pictures that were selected as stimuli for the association memory test. T-values are reported. All comparisons were not significant at α <0.05.

Set of pictures	Valence	Familiarity	Typicality	Discriminability of the image	Arousal	Spatial frequency	Brightness	Size

Changed pairs	0.05	0.05	0.04	0.43	0.35	0.01	0.29	0.47
Unchanged pairs	0.92	0.62	0.85	0.48	0.87	0.58	0.27	0.14

Table S6. Characteristics of the samples used for the FNC x PRS analysis grouped by cohort and group.

Cohort	Group	N	Mean age ± SD in years (range)	%Male
LIBD	yNC	81	22±2 (18:25)	50
	oNC	92	41±7 (30:56)	46
	ySIB	4	22±2 (18:25)	65
	oSIB	15	42±8 (30:60)	42
	oSCZ	40	40±8 (30:55)	65
UNIBA 1	yNC	255	22±2 (18:25)	40
	oNC	116	39±8 (30:60)	62
	ySIB	7	21±3 (18:25)	57
	oSIB	24	40±7 (30:59)	38
	oSCZ	46	38±7 (30:58)	60
UNIBA 2	yNC	85	22±2 (18:25)	36
	oNC	33	36±8 (30:60)	63
	yPSY	21	20±3 (15:25)	55
	oSCZ	21	39±6 (30:50)	61
PNC	cNC	40	11±2 (8:14)	43
	cPSY	12	12±1 (9:14)	86
	yNC	41	17±3 (15:21)	86
	yPSY	14	17±3 (15:20)	43
ABCD	cNC	3636	9.9±1 (9:11)	47
	cSIB/FHR	62	9.9±1 (9:11)	53
	cPSY	1238	9.8±1 (9:11)	24
UKB	oNC	2520	53±6 (40:60)	47

Table S7. Description of the sample size available for each cognitive measure included in the CFA. Numerosity, mean and standard deviations are reported for each group. Abbreviations: TMT = Trails Making Test; WAIS R = Wechsler Adult Intelligence Scale-Revised version; WMS = Wechsler Memory Scale.

UNIBA1	**yNC**	**oNC**	**ySIB**	**yPSY**	**oSIB**	**oSCZ**
TMT A (seconds)	308; 25±7	103; 26±9	12; 29±8	0	45; 40±24	56; 54±23
TMT B (seconds)	308; 57±23	103; 65±30	12; 75±28	0	45; 67±49	56; 97±46
WAIS R – Symbol search	291; 11±3	99; 10±3	8; 9±1	0	29; 8±3	34; 5±3
WMS - Logical Memory I	116; 7±3	48; 6±3	6; 4±3	0	13; 5±3	8; 4±3
WMS - Logical Memory II	116; 6±3	48; 4±1	6; 25±10	0	13; 3±1	8; 3±3
WMS - Verbal Pairs total	286; 18±3	102; 16±3	9; 16±3	0	33; 15±3	35; 10±5
WAIS R – Digit span forward	138; 8±2	53; 8±2	6; 6±1	0	11; 6±2	4; 5±2
WAIS R – Digit span backward	138; 8±2	53; 8±2	6; 7±2	0	11; 6±2	4; 4±1
1-Back (%)	329; 94±1	113; 93±10	11; 79±20	0	44; 76±20	69; 72±24
2-Back (%)	329; 78±17	112; 74±19	11; 60±21	0	42; 54±21	68; 50±17
3-Back (%)	215; 71±16	90; 64±18	0	0	3; 65±25	0
WCST – Perseverative errors	273; 7±10	92; 11±9	8; 11±7	0	28; 15±14	41; 22±20
WCST – Corrected responses	111; 70±26	47; 68±23	3; 60±41	0	7; 46±34	17; 44±32
WCST – Completed categories	287; 5±1	97; 5±1	10; 5±2	0	45; 4±2	64; 3±2
WMS – Visual Reproduction I	116; 4±1	48; 4±1	6; 4±2	0	13; 4±1	8; 2±1
WMS – Visual Reproduction II	116; 7±1	48; 7±1	6; 7±1	0	13; 6±2	8; 2±3
UNIBA1	**yNC**	**oNC**	**ySIB**	**yPSY**	**oSIB**	**oSCZ**
TMT A (seconds)	119; 23±7	56; 25±10	0	43; 28±8	0	24; 38±12
TMT B (seconds)	119; 54±26	56; 56±16	0	43; 70±34	0	24; 82±41
WAIS R – Symbol search	56; 12±8	11; 11±4	0	0	0	4; 5±2
WMS - Logical Memory I	99; 8±4	40; 8±3	0	17; 8±3	0	11; 4±5
WMS - Logical Memory II	99; 7±3	40; 8±3	0	17; 7±3	0	11; 4±3
WMS - Verbal Pairs total	101; 17±3	42; 16±4	0	36; 15±3	0	11; 11±3
WAIS R – Digit span forward	56; 8±1	9; 9±2	0	0	0	4; 6±2
WAIS R – Digit span backward	56; 7±2	9; 8±3	0	0	0	4; 5±1
1-Back (%)	119; 90±15	55; 90±10	0	44; 87±17	0	24; 72±23
2-Back (%)	117; 76±21	55; 70±17	0	42; 66±19	0	22; 56±15
3-Back (%)	117; 69±18	52; 62±19	0	16; 59±20	0	0
WCST – Perseverative errors	116; 7±9	53; 10±10	0	38; 9±8	0	16; 24±18

WCST – Corrected responses	117; 78±18	53; 71±24	0	38; 69±26	0	17; 55±26
WCST – Completed categories	120; 6±1	56; 5±1	0	44; 5±2	0	23; 4±2
WMS – Visual Reproduction I	99; 4±1	40; 4±1	0	17; 3±2	0	11; 3±1
WMS – Visual Reproduction II	99; 7±1	40; 6±2	0	17; 6±2	0	11; 2±2

Table S8. Characteristics of the samples used for the cognition analysis grouped by cohort and group.

Cohort	Group	N	Mean age ± SD in years (range)	%Male
LIBD	yNC	29	23±3 (19:25)	36
	oNC	50	43±7 (30:56)	48
	ySIB	0	/	/
	oSIB	6	40±9 (31:54)	66
	oSCZ	11	42±8 (30:52)	63
UNIBA 1	yNC	339	22±2 (18:25)	39
	oNC	113	38±7 (30:58)	61
	ySIB	11	21±2 (17:24)	36
	oSIB	44	40±6 (30:58)	41
	oSCZ	77	38±7 (30:58)	56
UNIBA 2	yNC	122	22±2 (17:25)	39
	oNC	56	37±7 (30:59)	57
	yPSY	44	20±3 (15:25)	50
	oSCZ	25	36±7 (30:50)	60

SI Figures

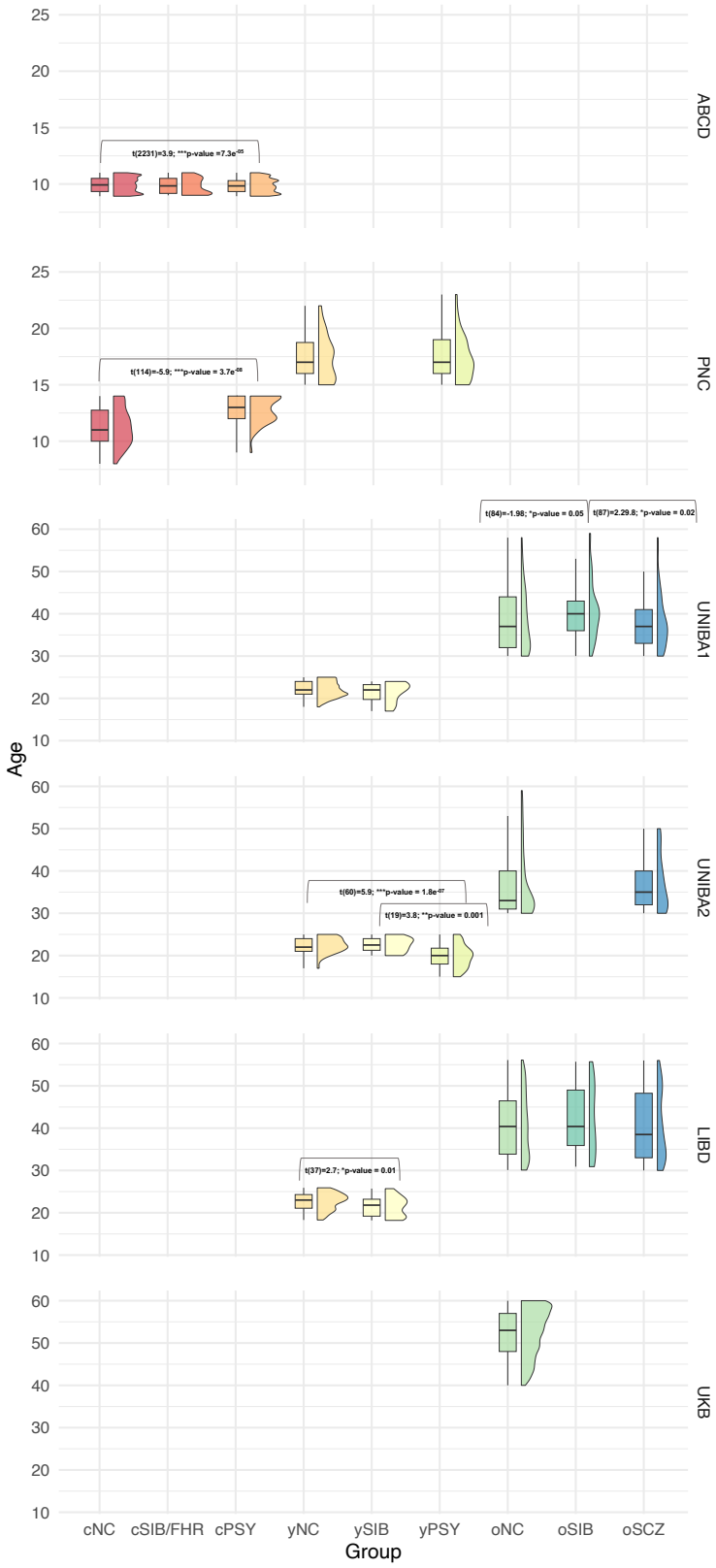
ABCD
PNC
UNIBA1
UNIBA2
LIBD
UKB
Age
Group
cNC
cSIB/FHR
cPSY
yNC
ySIB
yPSY
oNC
oSIB
oSCZ
t(2231)=3.9; ***p-value =7.3e-05
t(114)=-5.9; ***p-value = 3.7e-08
t(84)=-1.98; *p-value = 0.05
t(87)=2.29.8; *p-value = 0.02
t(60)=5.9; ***p-value = 1.8e-07
t(19)=3.8; **p-value = 0.001
t(37)=2.7; *p-value = 0.01

Figure S1. Box- and density plots showing age differences across age-stages. Different colors represent different groups: cNC (red), cSIB/FHR (orange), cPSY (light orange), yNC (dark yellow), ySIB (yellow), yPSY (light green), oNC (green), oSIB (dark green) and oSCZ (blue). Age differences between groups at the same age-stage within cohorts. t- and p-values are reported, and significance was set at $\alpha < 0.05$).

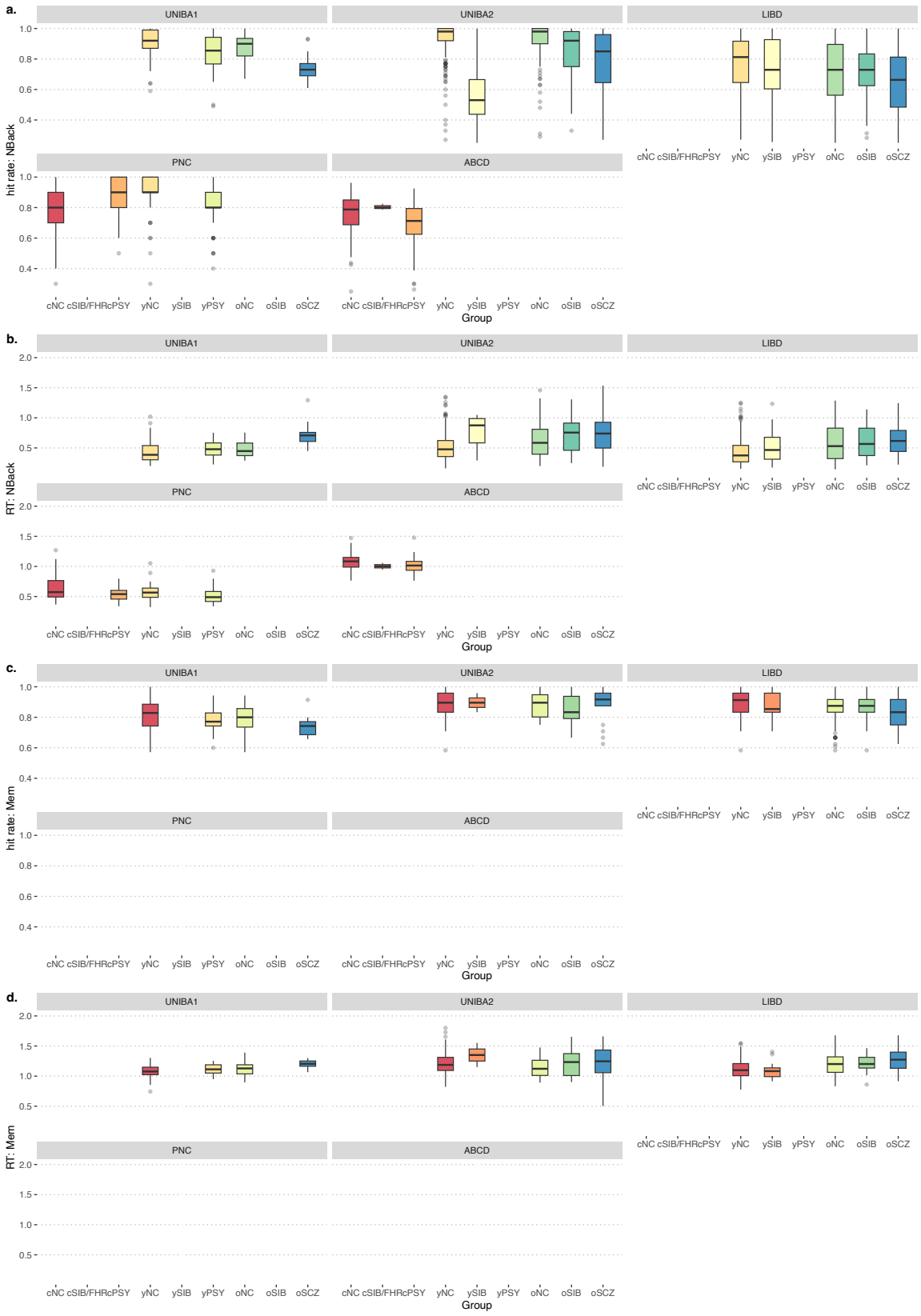
a.
UNIBA1
UNIBA2
LIBD
PNC
ABCD
hit rate: NBack
cNC cSIB/FHRcPSY yNC ySIB yPSY oNC oSIB oSCZ
Group
b.
RT: NBack
c.
hit rate: Mem
d.
RT: Mem

Figure S2. Boxplots showing differences across groups in terms of performance ($p<0.05$) grouped by cohort: (a) hit rate related to the working memory task (2-back for all cohorts); (b) RT (s) related to the working memory task. (c) hit rate related to the episodic memory tasks (PEAR for the LIBD and UNIBA1 cohorts and RISE for the UNIBA2 cohort); (d) RT (seconds) related to the episodic memory tasks; Note that episodic memory task was not acquired for the individuals included in PNC and ABCD.

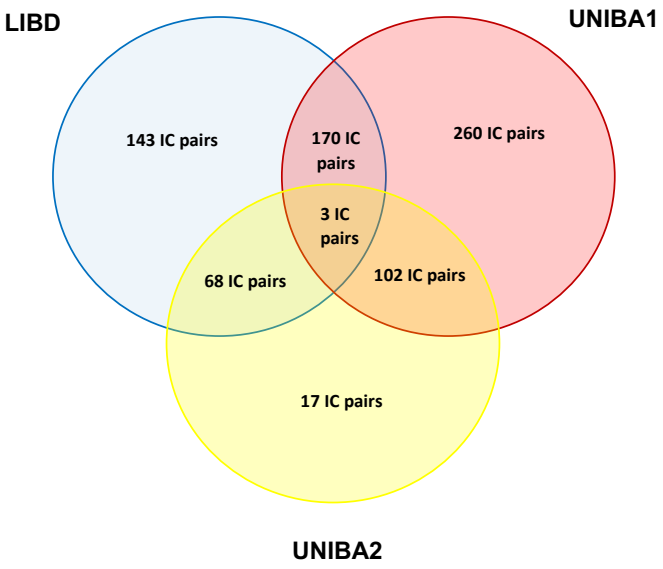

Figure S3. Venn diagram showing the accordance across the LIBD, UNIBA1, and UNIBA2 cohorts on age-group × session interactions. Results showed that a total of 406 IC pairs show a significant difference between yNC and oNC in the LIBD (blue circle), a total of 496 IC pairs show a significant difference between yNC and oNC in the UNIBA1 (red circle), and a total of 190 IC pairs show a significant difference between yNC and oNC in the UNIBA2 cohort (yellow circle).

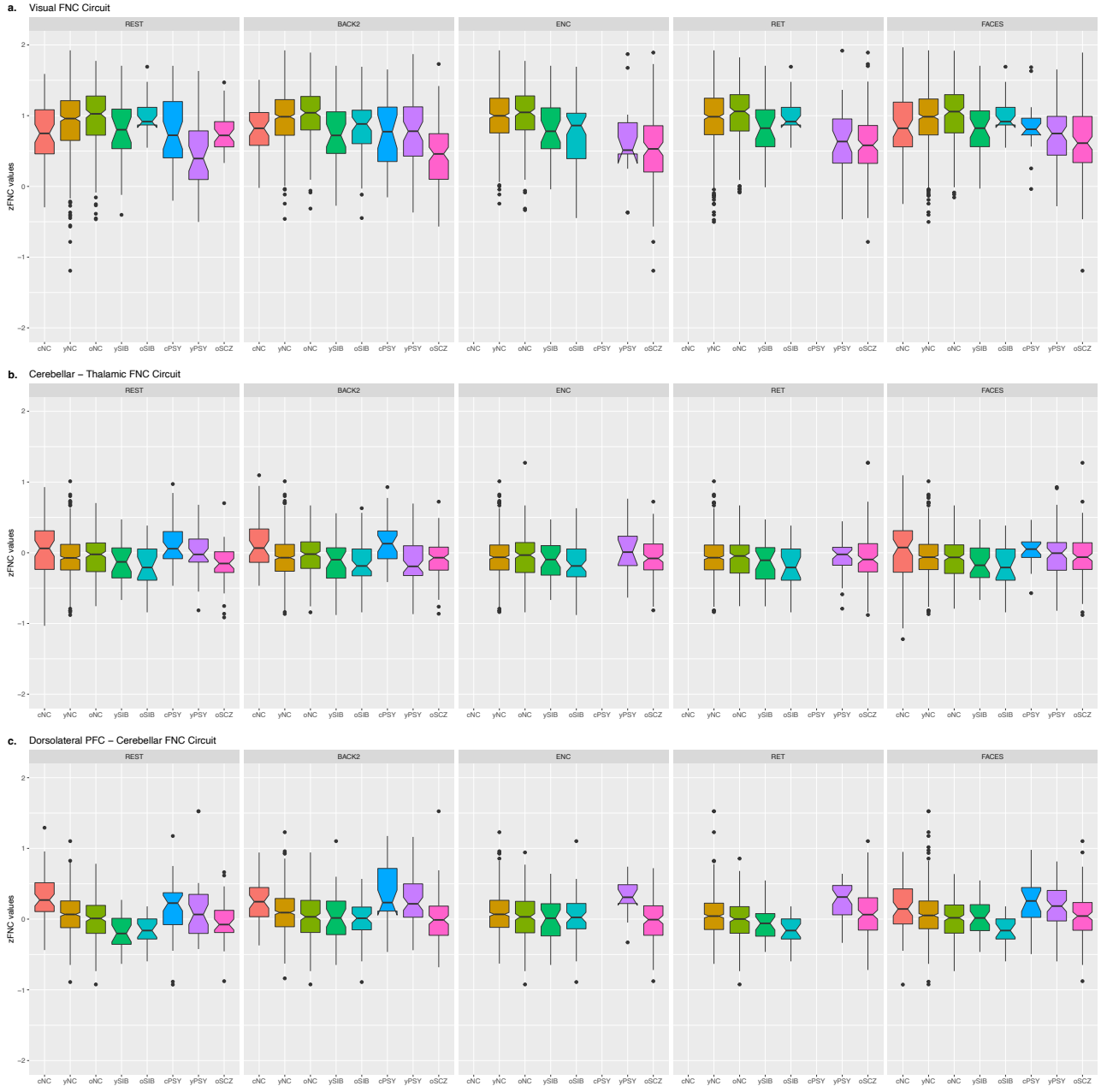

Figure S4. Boxplots showing the differences in terms of FNC between groups for each session among IC pairs resulted from age-group × session interactions.

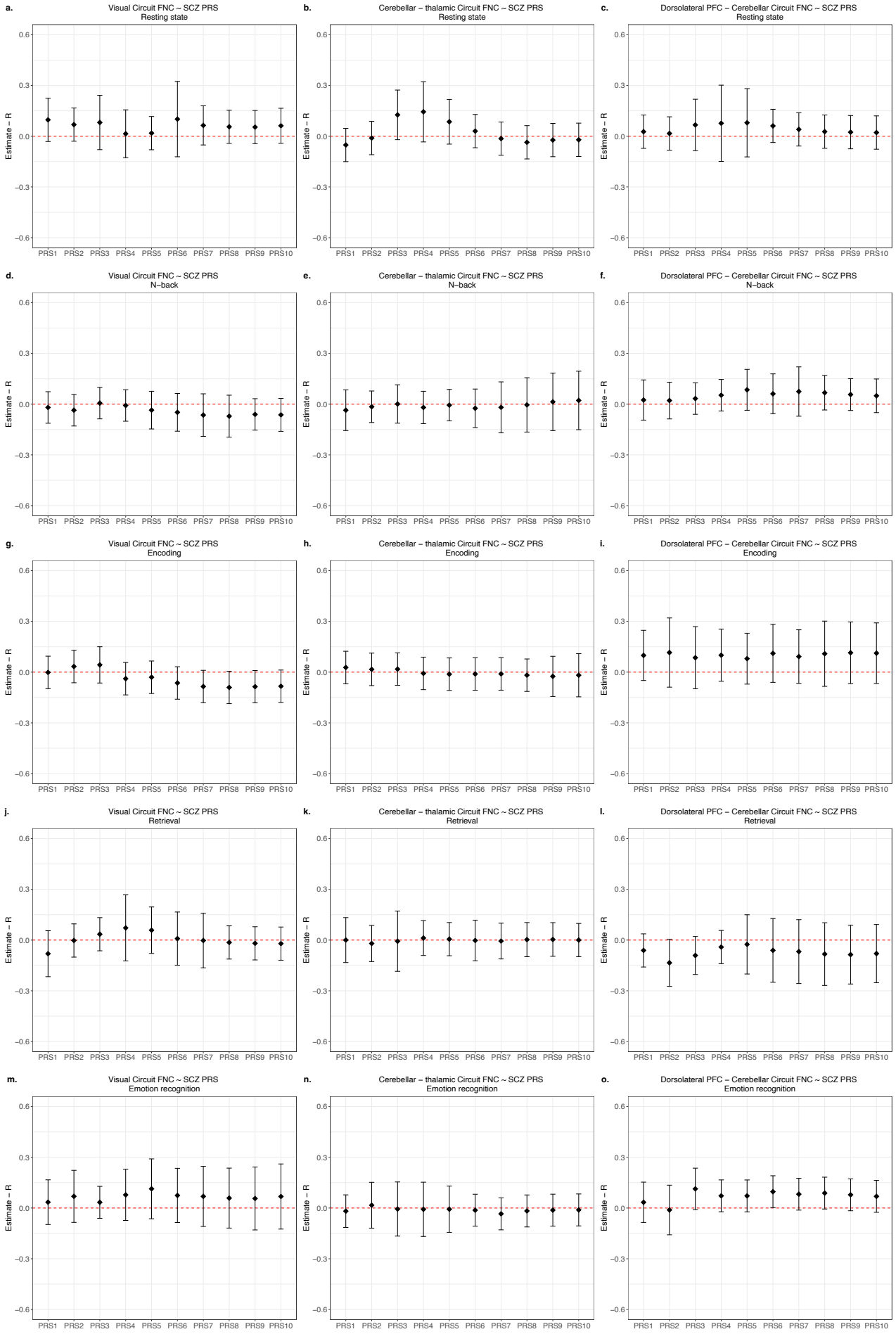
a.
Visual Circuit FNC ~ SCZ PRS
Resting state
b.
Cerebellar – thalamic Circuit FNC ~ SCZ PRS
Resting state
c.
Dorsolateral PFC – Cerebellar Circuit FNC ~ SCZ PRS
Resting state
d.
Visual Circuit FNC ~ SCZ PRS
N–back
e.
Cerebellar – thalamic Circuit FNC ~ SCZ PRS
N–back
f.
Dorsolateral PFC – Cerebellar Circuit FNC ~ SCZ PRS
N–back
g.
Visual Circuit FNC ~ SCZ PRS
Encoding
h.
Cerebellar – thalamic Circuit FNC ~ SCZ PRS
Encoding
i.
Dorsolateral PFC – Cerebellar Circuit FNC ~ SCZ PRS
Encoding
j.
Visual Circuit FNC ~ SCZ PRS
Retrieval
k.
Cerebellar – thalamic Circuit FNC ~ SCZ PRS
Retrieval
l.
Dorsolateral PFC – Cerebellar Circuit FNC ~ SCZ PRS
Retrieval
m.
Visual Circuit FNC ~ SCZ PRS
Emotion recognition
n.
Cerebellar – thalamic Circuit FNC ~ SCZ PRS
Emotion recognition
o.
Dorsolateral PFC – Cerebellar Circuit FNC ~ SCZ PRS
Emotion recognition
Estimate – R
0.6
0.3
0.0
−0.3
−0.6
PRS1 PRS2 PRS3 PRS4 PRS5 PRS6 PRS7 PRS8 PRS9 PRS10

Figure S5. Plots showing the association PRS × FNC for each session related to the three IC pairs in which we found a significant group × session interaction. The threshold pFDR <0.05 was considered on meta-analytic mixed effect model-derived p-values extracted across cohorts (C.I. 0.95). No significant association is reported.

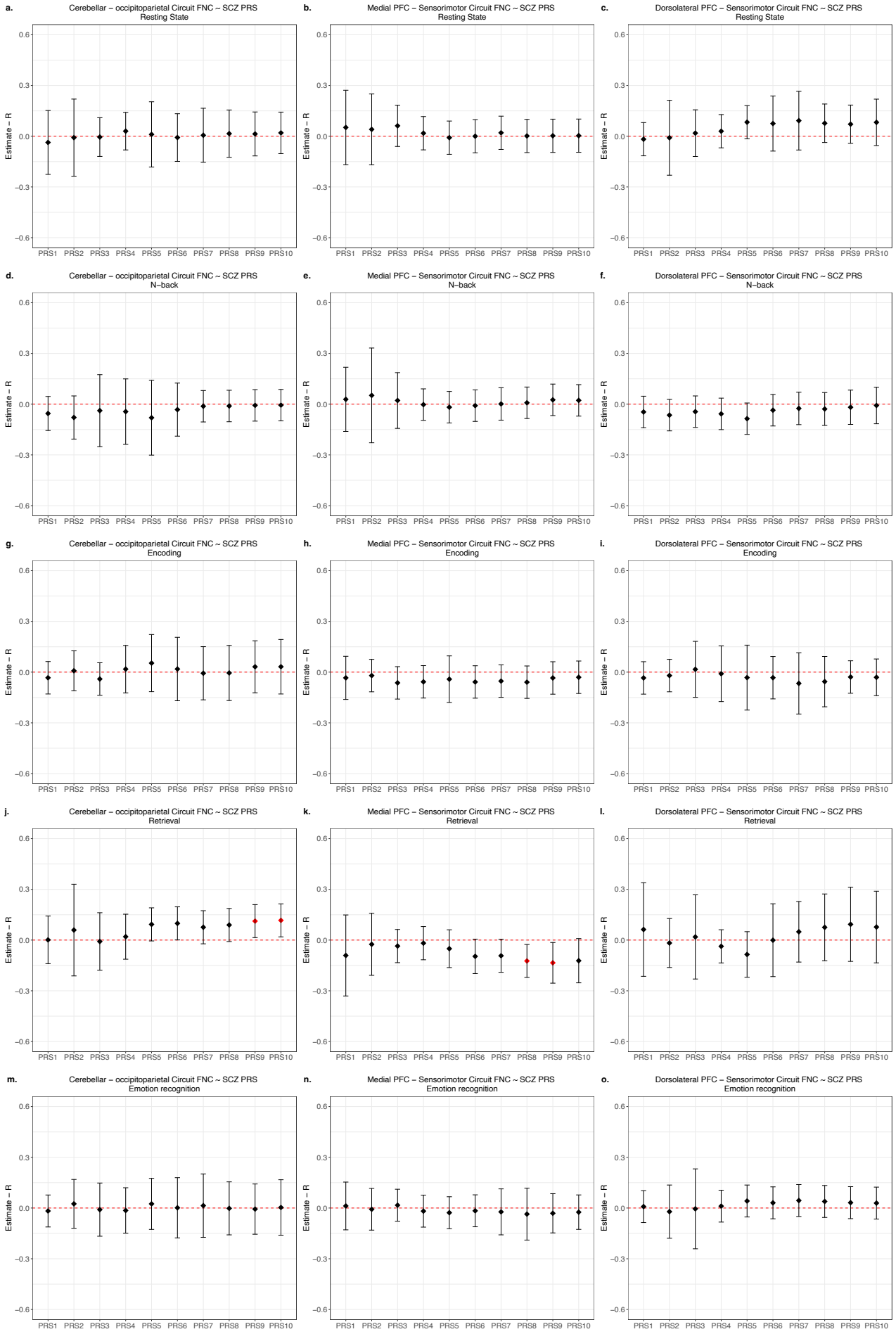
a.
Cerebellar – occipitoparietal Circuit FNC ~ SCZ PRS
Resting State
b.
Medial PFC – Sensorimotor Circuit FNC ~ SCZ PRS
Resting State
c.
Dorsolateral PFC – Sensorimotor Circuit FNC ~ SCZ PRS
Resting State
d.
Cerebellar – occipitoparietal Circuit FNC ~ SCZ PRS
N–back
e.
Medial PFC – Sensorimotor Circuit FNC ~ SCZ PRS
N–back
f.
Dorsolateral PFC – Sensorimotor Circuit FNC ~ SCZ PRS
N–back
g.
Cerebellar – occipitoparietal Circuit FNC ~ SCZ PRS
Encoding
h.
Medial PFC – Sensorimotor Circuit FNC ~ SCZ PRS
Encoding
i.
Dorsolateral PFC – Sensorimotor Circuit FNC ~ SCZ PRS
Encoding
j.
Cerebellar – occipitoparietal Circuit FNC ~ SCZ PRS
Retrieval
k.
Medial PFC – Sensorimotor Circuit FNC ~ SCZ PRS
Retrieval
l.
Dorsolateral PFC – Sensorimotor Circuit FNC ~ SCZ PRS
Retrieval
m.
Cerebellar – occipitoparietal Circuit FNC ~ SCZ PRS
Emotion recognition
n.
Medial PFC – Sensorimotor Circuit FNC ~ SCZ PRS
Emotion recognition
o.
Dorsolateral PFC – Sensorimotor Circuit FNC ~ SCZ PRS
Emotion recognition
Estimate – R
0.6
0.3
0.0
−0.3
−0.6
PRS1 PRS2 PRS3 PRS4 PRS5 PRS6 PRS7 PRS8 PRS9 PRS10

Figure S6. Plots showing the association PRS × FNC for each session related to the three IC pairs in which we found an age-related and risk-related effect. The threshold pFDR <0.05 was considered on meta-analytic mixed effect model-derived p-values extracted across cohorts (C.I. 0.95). Significant associations are reported in red.

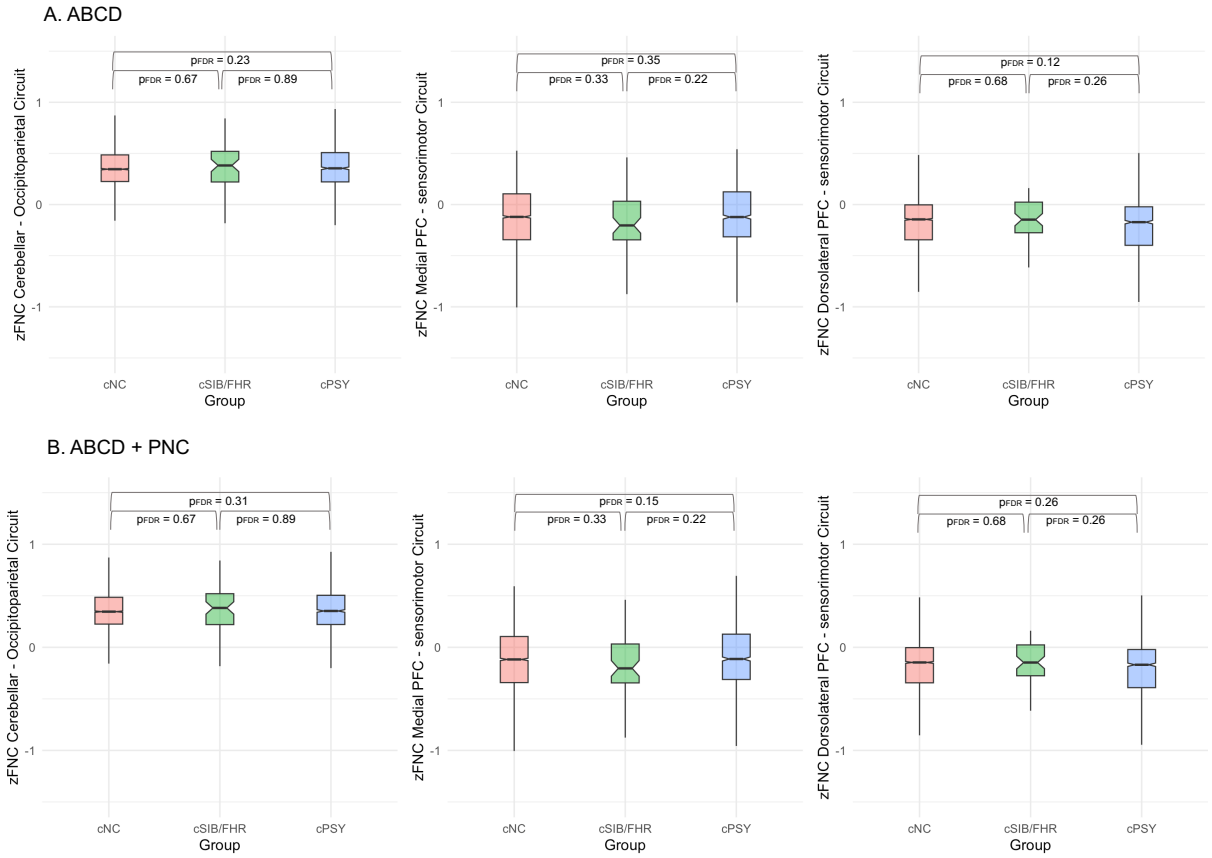

Figure S7. A) Risk-related FNC patterns extracted from the cerebellar-occipitoparietal circuit, the dorsolateral and medial PFC – sensorimotor circuits in cNC, cSIB/FHR, and cPSY from the ABCD cohort. B) Risk-related FNC patterns extracted in cNC, cSIB/FHR, and cPSY from the ABCD and PNC cohorts.

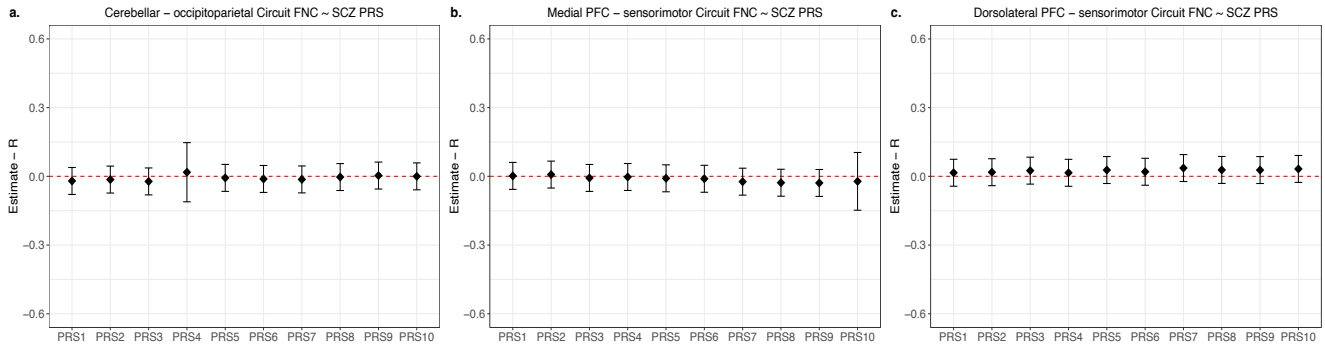

Figure S8. Plot showing the association between (a) cerebellar-occipitoparietal FNC, (b) medial and (c) dorsolateral PFC-sensorimotor FNC with PRS (1-10) across children in the PNC and ABCD. No significant result has been found (pFDR>0.05).

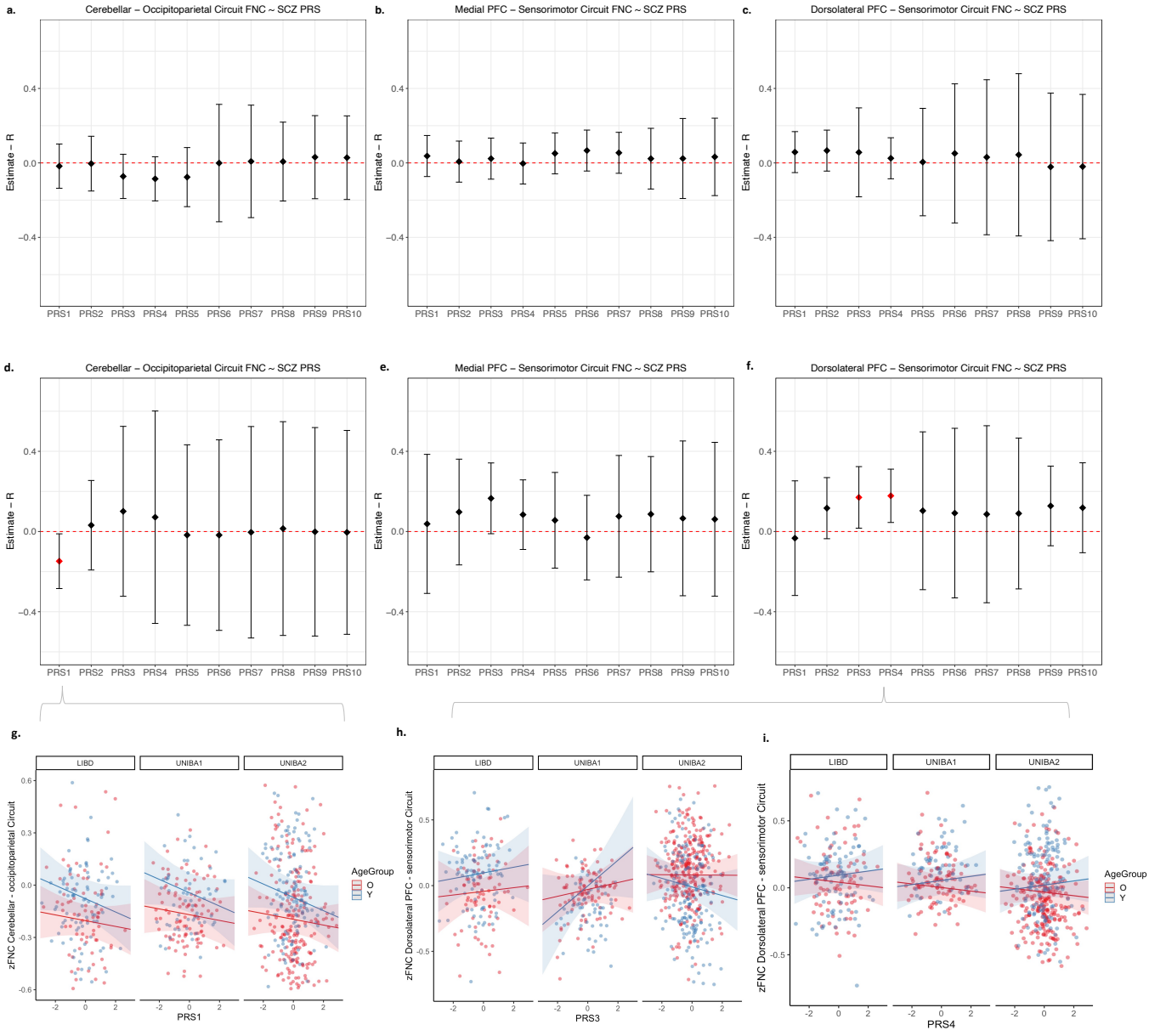

Figure S9. A-C. Plots showing the risk/diagnosis groups FNC × PRS interaction across sessions related to (a) the cerebellar-occipitoparietal circuit; (b) the medial PFC-sensorimotor circuit; (c) the dorsolateral PFC-sensorimotor circuit. D-F. Plots showing the age-groups FNC × PRS interaction across sessions related to (d) the cerebellar-occipitoparietal circuit; (e) the medial PFC-sensorimotor circuit; (f) the dorsolateral PFC-sensorimotor circuit. The threshold pFDR <0.05 was considered on meta-analytic mixed effect model-derived p-values extracted across cohorts (C.I. 0.95), accounting for multiple comparisons through Benjamini-Hochberg significance correction. Significant associations are reported in red. G. Scatterplot showing age-groups FNC × PRS1 interaction for each cohort in the cerebellar-occipitoparietal circuit (LIBD: Y, t=2.4; p=0.1; O, t=2.2;

p=0.02. UNIBA1: Y, t=2.5; p=0.02; O, t=2.1; p=0.04. UNIBA2: Y, t=2.6; p=0.02; O, t=2.2; p=0.05). H. Scatterplot showing age-groups FNC × PRS3 interaction for each cohort in the dorsolateral PFC-sensorimotor circuit (LIBD: Y, t=1.8; p=0.09; O, t=1.6; p=0.1. UNIBA1: Y, t=2.4; p=0.01; O, t=0.9; p=0.3. UNIBA2: Y, t=-2.1; p=0.05; O, t=0.7; p=0.6). H. Scatterplot showing age-groups FNC × PRS4 interaction for each cohort in the dorsolateral PFC-sensorimotor circuit (LIBD: Y, t=1.5; p=0.1; O, t=-1.2; p=0.1. UNIBA1: Y, t=0.9; p= 0.3; O, t=-1.1; p=0.2. UNIBA2: Y, t=1.2; p=0.3; O, t=-1.7; p=0.1).

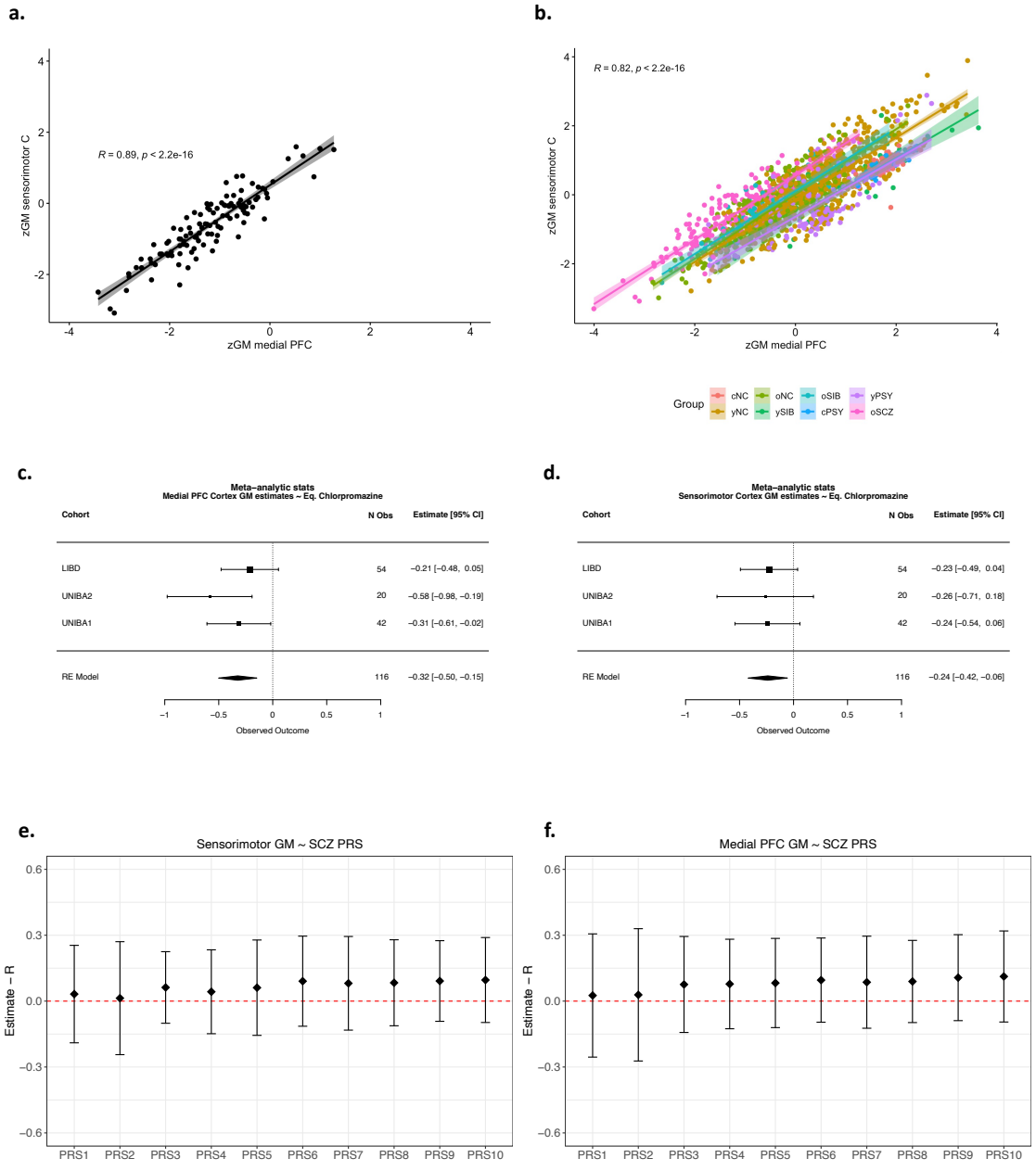

Figure S10. A-B. Scatterplots showing the association between medial PFC GM and sensorimotor cortex GM estimates in (a) oSCZ, and (b) all groups. C-D. Forest plots showing the association between Chlorpromazine Equivalents and (c) medial PFC GM, and (d) sensorimotor cortex GM. All results all reported at pFDR<0.05. E-F. Plots showing the association between medial PFC GM and PRS (1-10) and sensorimotor cortex GM and PRS (1-10).

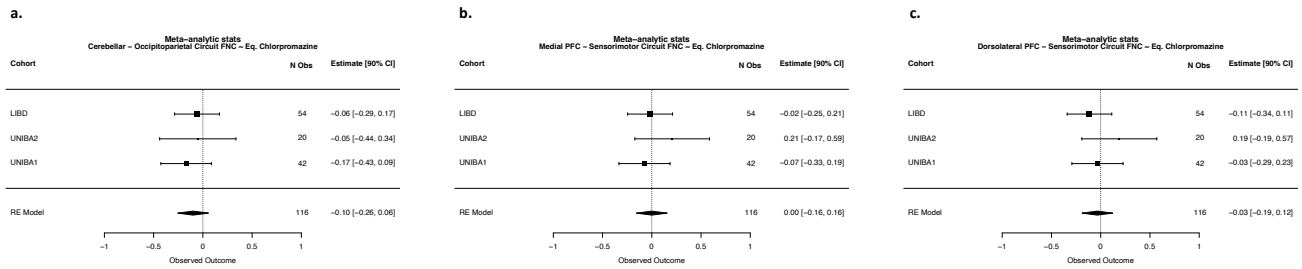

Figure S11. Plots showing the association between age- and risk-related FNC patterns and antipsychotic-based medication in a subsample of oSCZ with available treatment data (Chlorpromazine equivalents). The threshold $p<0.05$ was considered on meta-analytic mixed effect model-derived p-values extracted across cohorts (C.I. 0.95). No significant associations are reported.

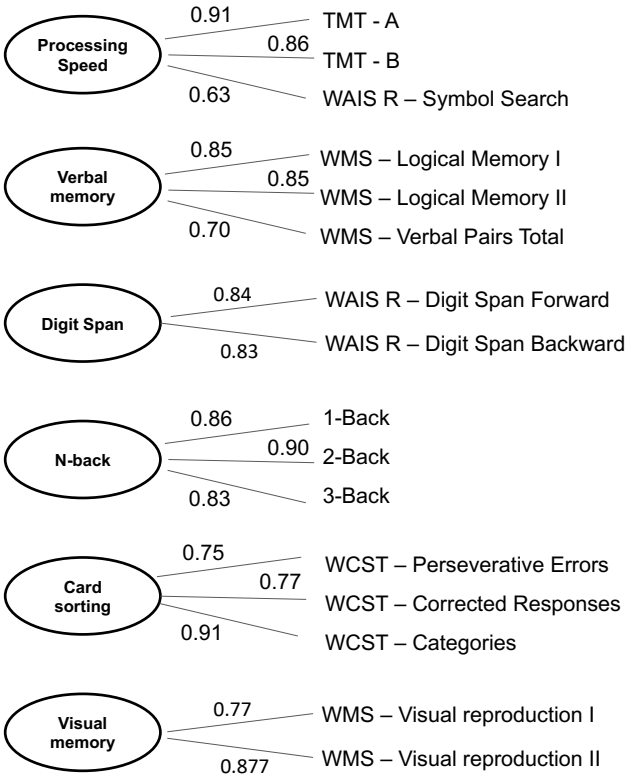

Figure S12. Final CFA solution. Loadings are from the UNIBA cohorts (N=831). Factors are represented in circles; the loading of each cognitive variable is indicated by grey lines. Abbreviations: TMT = Trails Making Test; WAIS R = Wechsler Adult Intelligence Scale-Revised version; WMS = Wechsler Memory Scale.

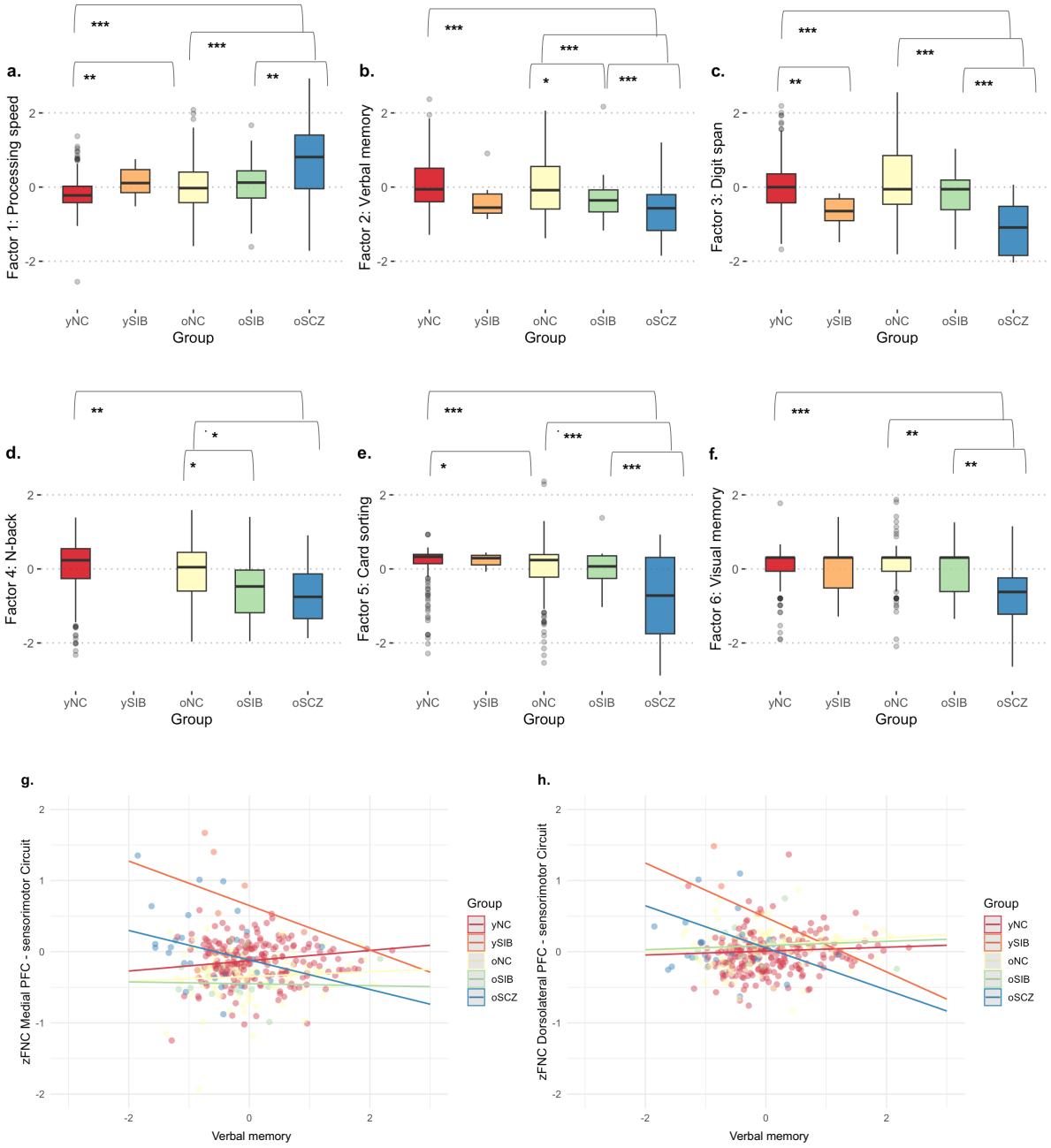

Figure S13. A-F. Boxplots show differences across groups in terms of cognitive performance defined by CFA as processing speed, verbal memory, digit span, N-back, card sorting, and visual memory. G. Scatterplot showing the association between medial PFC-sensorimotor circuit FNC and verbal memory (oSCZ: t=-2.41; p=0.01, ySIB: t =-2.1; p=0.05). H. Scatterplot showing the association between dorsolateral PFC-sensorimotor circuit FNC and verbal memory (oSCZ: t=-2.43; p=0.01, ySIB: t =-2.3; p=0.05).

SI References

1. C. C. Bell, DSM-IV: Diagnostic and Statistical Manual of Mental Disorders. *JAMA* **272**, 828-829 (1994).
2. M. E. Calkins *et al.*, The Philadelphia Neurodevelopmental Cohort: constructing a deep phenotyping collaborative. *J Child Psychol Psychiatry* **56**, 1356-1369 (2015).
3. H. Kobayashi *et al.*, A self-reported instrument for prodromal symptoms of psychosis: testing the clinical validity of the PRIME Screen-Revised (PS-R) in a Japanese population. *Schizophr Res* **106**, 356-362 (2008).
4. T. J. Miller *et al.*, The PRIME North America randomized double-blind clinical trial of olanzapine versus placebo in patients at risk of being prodromally symptomatic for psychosis. II. Baseline characteristics of the "prodromal" sample. *Schizophr Res* **61**, 19-30 (2003).
5. R. M. Xavier *et al.*, Characterizing Youth-Caregiver Concordance and Discrepancies in Psychopathology Symptoms in a US Community Sample. *Issues Ment Health Nurs* 10.1080/01612840.2022.2099494, 1-10 (2022).
6. C. Rosen, K. A. Chase, S. Perona-Garcelan, R. W. Marvin, R. P. Sharma, The psychometric properties of the DAIMON Scale, a translation from Spanish to English: An instrument to measure the relationship with and between voices. *Psychosis* **12**, 45-56 (2020).
7. D. M. Barch *et al.*, Demographic and mental health assessments in the adolescent brain and cognitive development study: Updates and age-related trajectories. *Dev Cogn Neurosci* **52**, 101031 (2021).
8. P. J. Ambrosini, Historical development and present status of the schedule for affective disorders and schizophrenia for school-age children (K-SADS). *J Am Acad Child Adolesc Psychiatry* **39**, 49-58 (2000).
9. N. R. Karcher *et al.*, Assessment of the Prodromal Questionnaire-Brief Child Version for Measurement of Self-reported Psychoticlike Experiences in Childhood. *JAMA Psychiatry* **75**, 853-861 (2018).
10. J. H. Callicott *et al.*, Physiological dysfunction of the dorsolateral prefrontal cortex in schizophrenia revisited. *Cereb Cortex* **10**, 1078-1092 (2000).
11. A. Bertolino *et al.*, Prefrontal dysfunction in schizophrenia controlling for COMT Val158Met genotype and working memory performance. *Psychiatry Res* **147**, 221-226 (2006).
12. J. D. Ragland *et al.*, Relational and Item-Specific Encoding (RISE): task development and psychometric characteristics. *Schizophr Bull* **38**, 114-124 (2012).
13. A. Di Giorgio *et al.*, Evidence that hippocampal-parahippocampal dysfunction is related to genetic risk for schizophrenia. *Psychol Med* **43**, 1661-1671 (2013).
14. R. Rasetti *et al.*, Altered hippocampal-parahippocampal function during stimulus encoding: a potential indicator of genetic liability for schizophrenia. *JAMA Psychiatry* **71**, 236-247 (2014).
15. H. Cao *et al.*, Altered Functional Subnetwork During Emotional Face Processing: A Potential Intermediate Phenotype for Schizophrenia. *JAMA Psychiatry* **73**, 598-605 (2016).
16. G. Blasi *et al.*, Functional variation of the dopamine D2 receptor gene is associated with emotional control as well as brain activity and connectivity during emotion processing in humans. *J Neurosci* **29**, 14812-14819 (2009).
17. P. Taurisano *et al.*, DAT by perceived MC interaction on human prefrontal activity and connectivity during emotion processing. *Soc Cogn Affect Neurosci* **8**, 855-862 (2013).
18. J. D. Ragland *et al.*, Working memory for complex figures: an fMRI comparison of letter and fractal n-back tasks. *Neuropsychology* **16**, 370-379 (2002).
19. R. C. Gur *et al.*, Brain activation during facial emotion processing. *Neuroimage* **16**, 651-662 (2002).
20. D. M. Barch *et al.*, Function in the human connectome: task-fMRI and individual differences in behavior. *Neuroimage* **80**, 169-189 (2013).
21. A. O. Cohen *et al.*, The Impact of Emotional States on Cognitive Control Circuitry and Function. *J Cogn Neurosci* **28**, 446-459 (2016).
22. M. D. Greicius, B. Krasnow, A. L. Reiss, V. Menon, Functional connectivity in the resting brain: a network analysis of the default mode hypothesis. *Proc Natl Acad Sci U S A* **100**, 253-258 (2003).
23. J. S. Damoiseaux *et al.*, Consistent resting-state networks across healthy subjects. *Proc Natl Acad Sci U S A* **103**, 13848-13853 (2006).
24. A. R. Mayer *et al.*, Functional imaging of the hemodynamic sensory gating response in schizophrenia. *Hum Brain Mapp* **34**, 2302-2312 (2013).
25. L. Fazio *et al.*, Transcriptomic context of DRD1 is associated with prefrontal activity and behavior during working memory. *Proc Natl Acad Sci U S A* **115**, 5582-5587 (2018).
26. B. L. Schlaggar *et al.*, Functional neuroanatomical differences between adults and school-age children in the processing of single words. *Science* **296**, 1476-1479 (2002).

27. B. J. Casey *et al.*, The Adolescent Brain Cognitive Development (ABCD) study: Imaging acquisition across 21 sites. *Dev Cogn Neurosci* **32**, 43-54 (2018).
28. Q. Chen *et al.*, Schizophrenia polygenic risk score predicts mnemonic hippocampal activity. *Brain* **141**, 1218-1228 (2018).
29. P. J. Lang, M. K. Greenwald, M. M. Bradley, A. O. Hamm, Looking at pictures: affective, facial, visceral, and behavioral reactions. *Psychophysiology* **30**, 261-273 (1993).
30. J. D. Ragland *et al.*, Functional and Neuroanatomic Specificity of Episodic Memory Dysfunction in Schizophrenia: A Functional Magnetic Resonance Imaging Study of the Relational and Item-Specific Encoding Task. *JAMA Psychiatry* **72**, 909-916 (2015).
31. F. Foroni, G. Pergola, G. Argiris, R. I. Rumiati, The FoodCast research image database (FRIDa). *Front Hum Neurosci* **7**, 51 (2013).
32. C. E. Stark, L. R. Squire, When zero is not zero: the problem of ambiguous baseline conditions in fMRI. *Proc Natl Acad Sci U S A* **98**, 12760-12766 (2001).
33. P. Ekman *et al.*, Universals and cultural differences in the judgments of facial expressions of emotion. *J Pers Soc Psychol* **53**, 712-717 (1987).
34. G. Blasi *et al.*, Preferential amygdala reactivity to the negative assessment of neutral faces. *Biol Psychiatry* **66**, 847-853 (2009).
35. A. R. Hariri, A. Tessitore, V. S. Mattay, F. Fera, D. R. Weinberger, The amygdala response to emotional stimuli: a comparison of faces and scenes. *Neuroimage* **17**, 317-323 (2002).
36. N. C. Ebner, M. Riediger, U. Lindenberger, FACES--a database of facial expressions in young, middle-aged, and older women and men: development and validation. *Behav Res Methods* **42**, 351-362 (2010).
37. D. M. Calhoun, G. M. Bucciarelli, L. B. Kats, R. K. Zimmer, P. T. J. Johnson, Noxious newts and their natural enemies: Experimental effects of tetrodotoxin exposure on trematode parasites and aquatic macroinvertebrates. *Toxicon* **137**, 120-127 (2017).
38. W. Lu, K. Dong, D. Cui, Q. Jiao, J. Qiu, Quality assurance of human functional magnetic resonance imaging: a literature review. *Quant Imaging Med Surg* **9**, 1147-1162 (2019).
39. M. L. Wood, R. M. Henkelman, Truncation artifacts in magnetic resonance imaging. *Magn Reson Med* **2**, 517-526 (1985).
40. Z. Song, N. Tustison, B. Avants, J. C. Gee, Integrated graph cuts for brain MRI segmentation. *Med Image Comput Comput Assist Interv* **9**, 831-838 (2006).
41. J. Ashburner, K. J. Friston, Unified segmentation. *Neuroimage* **26**, 839-851 (2005).
42. B. B. Avants, N. Tustison, G. Song, Advanced normalization tools (ANTS). *Insight j* **2**, 1-35 (2009).
43. J. D. Power, K. A. Barnes, A. Z. Snyder, B. L. Schlaggar, S. E. Petersen, Spurious but systematic correlations in functional connectivity MRI networks arise from subject motion. *Neuroimage* **59**, 2142-2154 (2012).
44. K. Friston, Learning and inference in the brain. *Neural Netw* **16**, 1325-1352 (2003).
45. B. B. Avants *et al.*, The pediatric template of brain perfusion. *Sci Data* **2**, 150003 (2015).
46. V. Fonov *et al.*, Unbiased average age-appropriate atlases for pediatric studies. *Neuroimage* **54**, 313-327 (2011).
47. K. Oishi, L. Chang, H. Huang, Baby brain atlases. *Neuroimage* **185**, 865-880 (2019).
48. J. E. Richards, C. Sanchez, M. Phillips-Meek, W. Xie, A database of age-appropriate average MRI templates. *Neuroimage* **124**, 1254-1259 (2016).
49. M. D. De Bellis *et al.*, Sex differences in brain maturation during childhood and adolescence. *Cereb Cortex* **11**, 552-557 (2001).
50. T. M. Evans, D. L. Flowers, E. M. Napoliello, G. F. Eden, Sex-specific gray matter volume differences in females with developmental dyslexia. *Brain Struct Funct* **219**, 1041-1054 (2014).
51. E. D. Gennatas *et al.*, Age-Related Effects and Sex Differences in Gray Matter Density, Volume, Mass, and Cortical Thickness from Childhood to Young Adulthood. *J Neurosci* **37**, 5065-5073 (2017).
52. B. B. Avants, C. L. Epstein, M. Grossman, J. C. Gee, Symmetric diffeomorphic image registration with cross-correlation: evaluating automated labeling of elderly and neurodegenerative brain. *Med Image Anal* **12**, 26-41 (2008).
53. F. Alfaro-Almagro *et al.*, Image processing and Quality Control for the first 10,000 brain imaging datasets from UK Biobank. *Neuroimage* **166**, 400-424 (2018).
54. Y. Du *et al.*, NeuroMark: An automated and adaptive ICA based pipeline to identify reproducible fMRI markers of brain disorders. *Neuroimage Clin* **28**, 102375 (2020).
55. Y. Du, Y. Fan, Group information guided ICA for fMRI data analysis. *Neuroimage* **69**, 157-197 (2013).
56. A. Fornito, J. Yoon, A. Zalesky, E. T. Bullmore, C. S. Carter, General and specific functional connectivity disturbances in first-episode schizophrenia during cognitive control performance. *Biol Psychiatry* **70**, 64-72 (2011).

57. L. Geerligs, C. Cam, R. N. Henson, Functional connectivity and structural covariance between regions of interest can be measured more accurately using multivariate distance correlation. *Neuroimage* **135**, 16-31 (2016).
58. J. W. Baurley *et al.*, Genome-Wide Association of the Laboratory-Based Nicotine Metabolite Ratio in Three Ancestries. *Nicotine Tob Res* **18**, 1837-1844 (2016).
59. S. Purcell *et al.*, PLINK: a tool set for whole-genome association and population-based linkage analyses. *Am J Hum Genet* **81**, 559-575 (2007).
60. T. S. W. G. o. t. P. G. Consortium, S. Ripke, J. T. Walters, M. C. O'Donovan, Mapping genomic loci prioritises genes and implicates synaptic biology in schizophrenia. *medRxiv* 10.1101/2020.09.12.20192922, 2020.2009.2012.20192922 (2020).
61. C. Schizophrenia Working Group of the Psychiatric Genomics, Biological insights from 108 schizophrenia-associated genetic loci. *Nature* **511**, 421-427 (2014).
62. K. Lange, *Mathematical and Statistical Methods for Genetic Analysis* (Springer New York, NY, 1997), https://doi.org/10.1007/978-1-4757-2739-5, pp. XII, 265.
63. S. R. Ellingson, D. W. Fardo, Automated quality control for genome wide association studies. *F1000Res* **5**, 1889 (2016).
64. S. Wright, Coefficients of Inbreeding and Relationship. *The American Naturalist* **54**, 330–338 (1922).
65. A. Gross, A. Tonjes, M. Scholz, On the impact of relatedness on SNP association analysis. *BMC Genet* **18**, 104 (2017).
66. B. Howie, J. Marchini, M. Stephens, Genotype imputation with thousands of genomes. *G3 (Bethesda)* **1**, 457-470 (2011).
67. O. Delaneau, J. Marchini, J. F. Zagury, A linear complexity phasing method for thousands of genomes. *Nat Methods* **9**, 179-181 (2011).
68. C. International Schizophrenia *et al.*, Common polygenic variation contributes to risk of schizophrenia and bipolar disorder. *Nature* **460**, 748-752 (2009).
69. S. W. Choi, P. F. O'Reilly, PRSice-2: Polygenic Risk Score software for biobank-scale data. *Gigascience* **8** (2019).
70. D. R. Weinberger, Implications of normal brain development for the pathogenesis of schizophrenia. *Arch Gen Psychiatry* **44**, 660-669 (1987).
71. S. K. Hill *et al.*, Neuropsychological impairments in schizophrenia and psychotic bipolar disorder: findings from the Bipolar-Schizophrenia Network on Intermediate Phenotypes (B-SNIP) study. *Am J Psychiatry* **170**, 1275-1284 (2013).
72. D. Dickinson, T. E. Goldberg, J. M. Gold, B. Elvevag, D. R. Weinberger, Cognitive factor structure and invariance in people with schizophrenia, their unaffected siblings, and controls. *Schizophr Bull* **37**, 1157-1167 (2011).
73. L. A. Antonucci *et al.*, Clinical and psychological factors associated with resilience in patients with schizophrenia: data from the Italian network for research on psychoses using machine learning. *Psychol Med* 10.1017/S003329172200294X, 1-12 (2022).
74. J. A. Moses, Jr., D. A. Pritchard, R. L. Adams, Neuropsychological information in the Wechsler Adult Intelligence Scale-Revised. *Arch Clin Neuropsychol* **12**, 97-109 (1997).
75. T. N. Tombaugh, Trail Making Test A and B: normative data stratified by age and education. *Arch Clin Neuropsychol* **19**, 203-214 (2004).
76. G. P. Prigatano, Wechsler Memory Scale: a selective review of the literature. *J Clin Psychol* **34**, 816-832 (1978).
77. J. Gallucci *et al.*, Greater individual variability in functional brain activity during working memory performance in Schizophrenia Spectrum Disorders (SSD). *Schizophr Res* **248**, 21-31 (2022).
78. J. Gallucci *et al.*, Longer illness duration is associated with greater individual variability in functional brain activity in Schizophrenia, but not bipolar disorder. *Neuroimage Clin* **36**, 103269 (2022).
79. C. Hawco, E. W. Dickie, G. Jacobs, Z. J. Daskalakis, A. N. Voineskos, Moving beyond the mean: Subgroups and dimensions of brain activity and cognitive performance across domains. *Neuroimage* **231**, 117823 (2021).

Group Author includes:

Ileana Andriola (Department of Translational Biomedicine and Neuroscience – University of Bari Aldo Moro, Bari, IT)
Lucia Mare (Department of Translational Biomedicine and Neuroscience – University of Bari Aldo Moro, Bari, IT)
Nicolò Parente (Department of Translational Biomedicine and Neuroscience – University of Bari Aldo Moro, Bari, IT)
Alessandra Raio (Department of Translational Biomedicine and Neuroscience – University of Bari Aldo Moro, Bari, IT)
Veronica Debora Toro (Department of Translational Biomedicine and Neuroscience – University of Bari Aldo Moro, Bari, IT)
Mario Altamura (Department of Mental Health, ASL Foggia, Foggia, IT; Department of Clinical and Experimental Medicine, University of Foggia, Foggia, IT)
Marimar Castrigno (Department of Mental Health, ASL Foggia, Foggia, IT)
Melania Difino (Department of Mental Health, ASL Foggia, Foggia, IT)
Flora Brudaglio (Department of Mental Health, ASL Barletta-Andria-Trani, Andria, IT)
Domenico Sabino Savino (Department of Mental Health, ASL Barletta-Andria-Trani, Andria, IT)
Rossana Vista (Department of Mental Health, ASL Barletta-Andria-Trani, Andria, IT)
Angela Carofiglio (Department of Mental Health, ASL Bari, Bari, IT)
Barbara Gelao (Department of Mental Health, ASL Bari, Bari, IT)
Marina Mancini (Department of Mental Health, ASL Bari, Bari, IT)
Alessandro Saponaro (Department of Mental Health, ASL Brindisi, Brindisi, IT)
Anna Manzari (Department of Mental Health, ASL Brindisi, Brindisi, IT)
Domenico Suma (Department of Mental Health, ASL Brindisi, Brindisi, IT)